C S P

The DOE Center of Excellence for the Synthesis and Processing of Advanced Materials

BASIC ENERGY SCIENCES
DIVISION OF MATERIALS SCIENCES
& ENGINEERING

Member Laboratories: Ames Laboratory, Argonne National Laboratory, Brookhaven National Laboratory, Idaho National Engineering and Environmental Laboratory, University of Illinois Frederick Seitz Materials Research Laboratory, Lawrence Berkeley National Laboratory, Lawrence Livermore National Laboratory, Los Alamos National Laboratory, National Renewable Energy Laboratory, Oak Ridge National Laboratory, Pacific Northwest National Laboratory, and Sandia National Laboratories

Research Briefs

For questions and additional information contact:

George A. Samara
Sandia National Laboratories/NM
Phone: (505) 844-6653
Fax: (505) 844-4045
E-mail: gasamar@sandia.gov

C S P

The DOE Center of Excellence for the Synthesis and Processing of Advanced Materials

BASIC ENERGY SCIENCES
DIVISION OF MATERIALS SCIENCES
& ENGINEERING

Research Briefs

October 2004

Table of Contents

Research Briefs

Table of Contents

Preface

This publication, *Research Briefs*, is designed to inform present and potential customers and partners of the DOE Center of Excellence for the Synthesis and Processing of Advanced Materials (CSP) about significant advances resulting from Center-coordinated research. The format for *Research Briefs* is an easy-to-read, not highly technical, concise presentation of the accomplishments. Each *Brief* provides a statement of the motivation for the research followed by a description of the accomplishment and its significance.

The Center is a distributed center for promoting coordinated, collaborative research partnerships related to the synthesis and processing of advanced materials. It was established by the Department of Energy's Division of Materials Sciences and Engineering, Office of Basic Energy Sciences and the DOE Laboratories in recognition of the enabling role of materials synthesis and processing to numerous materials fabrication- and manufacturing-intensive technologies. The participants include investigators from 12 DOE national laboratories, universities and the private sector. The Center has a technology perspective provided by a Technology Steering Group.

By bringing together synergistic activities and capabilities in selected focus areas of materials synthesis and processing, the Center's goal is to be a vehicle for providing added value and making impact. The Center is also allowing better coordinated strategic planning by the Division of Materials Sciences and Engineering and the Laboratories and faster response time to special needs and opportunities. Additionally, the Center is serving as a model of R and D integration within the Department of Energy as well as a model of cooperation and collaboration among the participating institutions.

The overall objective of the Center is,

To enhance the science and engineering of materials synthesis and processing in order to meet the programmatic needs of the Department of Energy and to facilitate the technological exploitation of materials.

Synthesis and processing (S&P) are those essential elements of Materials Science and Engineering (MS&E) that deal with (1) the assembly of atoms or molecules to form materials, (2) the manipulation and control of the structure at all levels from the atomic to the macroscopic scale, and (3) the development of processes to produce materials for specific applications. Clearly, S&P represent a large area of MS&E that spans the range from fundamental research to technology. The goal of basic research in this area ranges from the creation of new materials and the improvement of the properties of known materials, to the understanding of such phenomena as diffusion, interfacial phenomena, crystal growth, sintering, phase transitions, to the development of novel diagnostic, modeling and processing approaches, etc. On the applied side, the goal of S&P is to translate scientific results into useful materials by developing processes capable of producing high quality, cost-effective products.

The technical emphasis of the Center is on a number of focused multilaboratory projects which draw on the complementary strengths of the member institutions in their ongoing research programs. These projects were selected on the basis of the following criteria:

- scientific excellence
- clear relationship to energy technologies
- involvement of several laboratories
- existing or potential partnerships with DOE Technologies-funded programs
- existing or potential "in-kind" partnerships with industry

Each Project is coordinated by a knowledgeable representative from one of the participating laboratories. The Projects covered in this issue of *Research Briefs* and their Coordinators are listed in the accompanying table (p. 7). A few selected accomplishments from each of the Projects are presented. An Executive Summary provides highlights of these accomplishments organized by Project. Readers are encouraged to contact any of the Coordinators for information about the Center and its accomplishments.

The newest Center project is *Spin-Polarized Transport in Complex Oxides* which started at the beginning of FY2004. Center Projects are graduated after achieving their objectives, but no later than five years after start.

George A. Samara
October 2004

The Center's Member Laboratories

The member laboratories of the Center are:

- Ames Laboratory (Ames)
- Argonne National Laboratory (ANL)
- Brookhaven National Laboratory (BNL)
- Idaho National Engineering and Environmental Laboratory (INEEL)
- University of Illinois Frederick Seitz Materials Research Laboratory (UI/MRL)
- Lawrence Berkeley National Laboratory (LBNL)
- Lawrence Livermore National Laboratory (LLNL)
- Los Alamos National Laboratory (LANL)
- National Renewable Energy Laboratory (NREL)
- Oak Ridge National Laboratory (ORNL)
- Pacific Northwest National Laboratory (PNNL)
- Sandia National Laboratories (SNL)

Membership of the Technology Steering Group

Member	Affiliation
Prof. L. Eric Cross	Pennsylvania State University
Dr. David W. Johnson, Jr.	Stevens Inst of Technology
Dr. Hylan B. Lyon	Marlow Industries
Dr. Christian Mailhot	DOE/Defense Programs; Lawrence Livermore National Laboratory
Dean Paul S. Peercy	University of Wisconsin
Dr. Udaya Rao	DOE/Fossil Energy
Dr. John Stringer	Electric Power Research Institute (EPRI)
Dr. Arthur Yang	Arthur Yang Industrial Science and Technology Network, Inc.

Center Projects Covered In This Issue Of *Research Briefs* and Their Coordinators

Project	Coordinator(s)
Isolated and Collective Phenomena in Nanocomposite Magnets	Samuel D. Bader (ANL) Phone: (630) 252-4960 E-mail: bader@anl.gov
Smart Structures Based on Electroactive Polymers	Gregory J. Exarhos (PNNL) Phone: (509) 376-4125 E-mail: greg.exarhos@pnl.gov
Nanoscale Phenomena in Perovskite Thin Films	Orlando Auciello (ANL) Phone: (630) 252-1685 E-mail: auciello@anl.gov and Paul G. Clem (SNL/NM) Phone: (505) 845-7544 E-mail: pgclem@sandia.gov
Carbon-Based Nanostructured Materials	John Carlisle (ANL) Phone: (630) 252-3520 E-mail: carlisle@anl.gov and Thomas Friedmann (SNL/NM) Phone: (505) 844-6684 E-mail: tafried@sandia.gov
Granular Flow and Kinetics	Rodney Fox (Ames) Phone: (515) 294-9104 E-mail: rofox@iastate.edu
Experimental and Computational Lubrication at the Nanoscale	Steve Granick (UI/MRL) Phone: (217) 333-5720 E-mail: sgranick@uiuc.edu
Spin-Polarized Transport in Complex Oxides	John F. Mitchell (ANL) Phone: (630) 252-5852 E-mail: mitchell@anl.gov
Overall Center Coordinator	George A. Samara (SNL/NM) Phone: (505) 844-6653 E-mail: gasamar@sandia.gov

Executive Summary

The *Research Briefs* presented in this publication are intended to inform the Center's present and potential customers and partners about significant advances resulting from Center-coordinated research. Selected accomplishments from each project are presented. This Executive Summary states the overall objective of each project followed by highlights of the accomplishments presented later in more detail.

Isolated and Collective Phenomena in Nanocomposite Magnets

Objective

Develop improved understanding of magnetic properties as well as improved magnetic materials using nanoscale mixtures of hard magnets, soft magnets and non-magnetic materials.

Highlights

- Single crystal and powder diffraction techniques were combined with resonant scattering of circularly polarized x-rays to separate the magnetic responses of atoms of the same chemical species in inequivalent crystallographic sites or dissimilar crystal phases. (p. 16)

- A method was developed to fully characterize the magnetic properties of high energy product nanostructured permanent magnets from measurement of a simple demagnetization curve. The method is based on the full numerical solution minimizing the energy of a random collection of interacting unaxial magnetic particles in the presence of an applied magnetic field. (p. 18)

- Resonant x-ray scattering techniques have been developed at the Advanced Light Source to obtain direct information on interparticle dipolar interactions in magnetic nanoparticle assemblies. These techniques were used to study interparticle correlations in dense assemblies of 9-nm Co particles in both the cubic and hexagonal phases. (p. 20)

Smart Structures Based on Electroactive Polymers

Objective

Develop a framework for the rational design of self-assembled nanostructured block copolymers that offer significant advantages over conventional materials for the active regulation of transport phenomena.

Highlights

- Innovative approaches have been developed to synthesize copolymers that exhibit reversible volume changes when subjected to heat, light, applied electric field or solution chemistry. (p. 22)

- Hydrogel based hydrophilic polymer templates that exhibit reversible volume changes in a physiological temperature range have been developed. Biological applications include real-time sensing of large molecules in solution and the controlled release or sequestration of proteins. (p. 24)

- It is demonstrated that enhanced solution hydrophilicity can direct block copolymer nanofibers to self-align and subsequently assemble into fiber bundles under suitable pH conditions. Such bundles exhibit waveguiding properties and photoluminesce under short wavelength excitation. (p. 26)

Nanoscale Phenomena in Perovskite Thin Films

Objective

Develop the scientific basis for controlling nucleation, growth and strain in ferroelectric perovskite thin films.

Highlights

- Novel ($Ti_xAl_{1-x}O_y$) thin film alloys with high dielectric constants and low leakage were deposited on Si substrates. They appear to be potential candidates for high dielectric constant dielectric gates for metal/oxide/semiconductor structures. (p. 28)

- $LiNbO_3$ has been shown to display an unusual dynamical response with both order-disorder and displacive dynamics. Moreover, the transition temperatures for the two distinct contributors to the ferroelectric response were found to be very different from each other. (p. 30)

- Results on a superlattice consisting of alternating layers of the ferroelectric $KNbO_3$ and the paraelectric $KTaO_3$ have revealed an antiferroelectric and not ferroelectric ordering of the $KNbO_3$ dipoles when the $KNbO_3$ layers are on the order of one unit cell thick. (p. 32)

Carbon-Based Nanostructured Materials

Objective

Advance the science and technology of carbon-based materials that will lead to the development of new generations of MEMS and NMES devices.

Highlights

- Novel multifunctional carbon nanofiber scanning probe tips with controlled length, shape, aspect ratio and tip sharpness have been grown. (p. 34)
- Simultaneous synthesis of ultra-nanocrystalline diamond and carbon nanotubes has been achieved to form a covalently-bonded hybrid material: a nanocomposite of diamond and carbon nanotubes. (p. 36)
- Intense thermionic field emission has been observed from ultra-nanocrystalline diamond-coated tip structures. Field-enhanced electrons emitted from a tip result in higher current densities at the collector than those emitted from a flat surface. (p. 38)

Granular Flow and Kinetics

Objective

Develop constitutive relationships for the dynamic response of granular materials capturing the breadth of granular kinetics and flows in fundamental ways.

Highlights

- A new type of Couette shear cell combined with simulations have enabled detailed study of the development of the shear zone in dense granular flows. The simulations provide more detailed information than the experiments on the evolution of the stresses in the sheared granular pack. (p. 40)

- The nature of avalanches in thin layers on inclined planes has been demonstrated to depend sensitively on the type of material in the avalanche - surprising new results. (p. 42)

- Electrostatic driving of granular media is shown to provide precise and controlled characterization of granular ensembles. New insights into coarsening and dipolar interactions between particles are revealed by the data. (p. 44)

Experimental and Computational Lubrication at the Nanoscale

Objective

Develop a scientific understanding of lubrication and strategies to control tribology at the nanoscale capitalizing on recent advances in nanoprobe, theoretical and computational methods.

Highlights

- Use of a nanotribological model in molecular dynamics simulations combined with experimental measurements have provided new insights into the structure and friction dynamics of nanoconfined hydration layers. (p. 46)

- It has been demonstrated that the optoelectronic properties of a conjugated polymer can be modified by combined alignment of chain conformations by shear and nanoconfinement. It is suggested that the approach can be used to induce novel chemical reactions. (p. 48)

- An integrated, multi-scale study of friction using both AFM and MEMS - level experiments has revealed new insights into friction, adhesion and wear in MEMS devices. (p. 50)

Spin-Polarized Transport in Complex Oxides

Objective

To understand, control, and manipulate spin-polarized transport within and between highly spin-polarized oxides in order to create and exploit spintronic functionality.

Highlights

- Using a combination of surface sensitive x-ray and tunneling probes shows that, for the quasi-two-dimensional bilayer manganites $La_{2-2x}Sr_{1+2x}Mn_2O_7$, only the outermost Mn-O bilayer loses spin polarization (SP). This 1-nm thick intrinsic nanoskin is an insulator with no long-range FM order, while the next bilayer displays the full SP of the bulk, demonstrating natural assembly of 2/3 of a magnetic tunnel junction. (p. 52)

- Nanostructuring of 1-D wires of LSMO in an LCMO matrix has been achieved by a novel MBE growth technique. The transport is highly anisotropic (parallel to the wires versus perpendicular), and the metal insulator transition is substantially suppressed relative to the ferromagnetic Curie point. (p. 54)

- Ultrasharp steps in magnetization of $Pr_{0.65}(Ca_ySr_{1-y})_{0.35}MnO_3$ films demonstrates two of the key issues in CMR manganites to be addressed for spin-polarization: phase competition and interfacial strain. A time dependence to the appearance of steps suggests this strain self-organizes before being relieved by the magnetic field. (p. 56)

Research Briefs

Understanding our Best Permanent Magnets: Site- and Phase-Specific Magnetism in $Nd_2Fe_{14}B$ and its Composites

D. Haskel, J. Lang, Z. Islam, G. Srajer, J.S. Jiang *and* ***S. D. Bader,*** *Argonne National Laboratory*
Bao-Min Ma, *Magnequench International, Inc.*
Paul Canfield, *Ames Laboratory*

Motivation—Magnetic hardness, *i.e.*, the ability of some materials to remain magnetized even under the application of strong demagnetizing fields, is a key property of permanent magnets. It originates at the atomic level and it is determined by interactions between electronic orbitals at atomic sites and the electric field of their surrounding atoms. This interaction results in a preferred orientation of the magnetic moments relative to the material's crystalline axes. Altering this preferred arrangement is energy-costly, resulting in the desired magnetic stability. It is well established that the best permanent magnets gain this stability mostly through the rare-earth sites (Nd in NdFeB, and Sm in SmCo) but progress in gaining a deep understanding of this effect is masked by the simultaneous presence of more than one crystalline environment around rare-earth sites, or more than one crystalline phase in exchange-coupled nanocomposites. The goal is to develop x-ray based techniques that allow separating the magnetic responses of atoms of the same chemical species in inequivalent crystal sites or dissimilar crystal phases.

Accomplishment—Single crystal and powder diffraction techniques were combined with resonant scattering of circularly polarized x-rays to study the magnetic response of the two inequivalent Nd crystal sites in $Nd_2Fe_{14}B$ single crystal, as well as the Fe magnetism in both phases of $Nd_2Fe_{14}B/\alpha$-Fe exchange-coupled nanocomposites. By working under specially chosen Bragg diffraction conditions, contributions from either one or the other inequivalent Nd crystal sites in $Nd_2Fe_{14}B$ can be separated. In addition, by using phase-specific Bragg reflections of $Nd_2Fe_{14}B$ and α-Fe phases, magnetic contributions from Fe in either phase of a nanocomposite can be separated. The use of circularly polarized x-rays at characteristic Nd or Fe resonant energies gives sensitivity to their magnetic moments and response to applied magnetic fields. Experiments were carried out at sector 4 of the Advanced Photon Source at ANL on high quality single crystals of $Nd_2Fe_{14}B$ crystals grown at Ames Laboratory and nanocomposite exchange magnets developed at Magnequench Inc. Figure 1 shows hysteresis loops measured for each of the Nd crystal sites. The displayed flipping ratios are obtained from the asymmetry in the diffracted intensity for opposite x-ray helicities, which is proportional to the Nd magnetic moment. The results clearly indicate that Nd (1) sites are magnetically harder than Nd (2) sites, as the former require a larger demagnetizing field to nucleate a reversal of their magnetic moments.

Significance—The stability of $Nd_2Fe_{14}B$ against demagnetizing fields appears to have its origin predominantly at only one of the two Nd crystal sites, namely the Nd (1) site. Since its crystalline environment is known, the realization of new generations of stronger permanent magnets by tailoring the crystalline environment of rare-earth sites presents an exciting opportunity. The ability of these newly developed techniques to separate the magnetic responses of elements of the same chemical species in coexisting different crystalline environments adds greatly to our ability to characterize complex permanent magnetic materials.

Contact: D. Haskel, Argonne National Laboratory
Phone: (630) 252-7758, Fax: (630) 252-7392, E-mail: haskel@aps.anl.gov

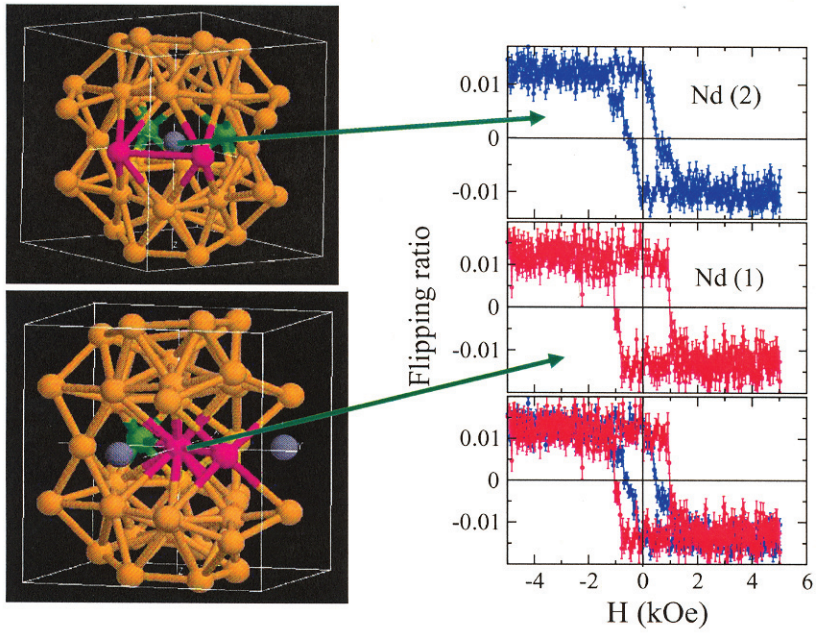

Figure 1. Coexisting Nd crystalline environments in $Nd_2Fe_{14}B$ permanent magnet (left). Site-specific Nd L_2-edge hysteresis loops (right). The crystalline environment at the Nd (1) site results in its higher stability against demagnetizing fields.

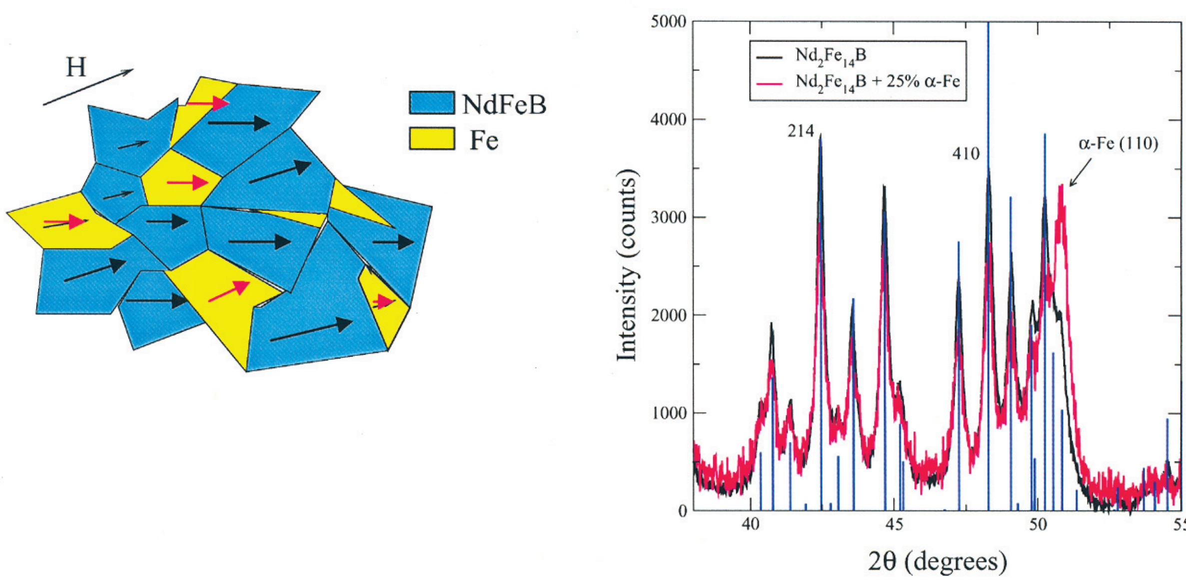

Figure 2. (Left) Schematic of exchange-coupled nanocomposite with hard and soft magnetic phases. Magnetic contributions from Fe atoms in either phase can be separated by selecting appropriate Bragg diffraction conditions (right) and using circularly polarized x-rays at Fe K-edge resonance to couple to their magnetic moments.

Exchange Enhanced Nanocrystalline Hard Magnets

R. W. McCallum *and* ***M. J. Kramer,*** *Ames Laboratory*
L. H. Lewis, *Brookhaven National Laboratory*
B.-M. Ma, *Magnequench International, Inc.*
J. E. Shield, *University of Nebraska - Lincoln*

Motivation—Nanostructured permanent magnet materials provide a performance enhancement of up to 50% over those with less controlled microstructures due to the exchange coupling between the nanograins. This interaction results in collective behavior of all the grains in the magnet compared to the independent behavior of the grains in a conventional magnet. While the overall nanostructure of the magnet may be characterized, it is not possible to characterize the intrinsic properties of the individual grains; thus it is very difficult to quantify the exchange coupling between grains. The investigation of various means of characterizing these properties within this CSP project has resulted in a simple model for interacting uniaxial ferromagnets which yields a quantitative description of the magnetic material's properties and allows the interaction and intrinsic properties to be determined from a simple measurement of the hysteresis loop.

Accomplishment—In the study of exchange enhanced or exchange spring isotropic permanent magnets, three quantities are of primary interest: the saturation magnetization, M_S, the magnetic anisotropy field, H_a and the degree of coupling between the individual grains of the sample. The most frequently used metric for the interaction strength in exchange-enhanced magnets is the ratio of the remanent magnetization to the saturation magnetization (M_R/M_S). The standard method for the determination of the saturation magnetization requires measurements in magnetic fields which are only available in a few specialized laboratories, while measurement of H_a requires single crystals. We have demonstrated that all three quantities may be derived from fitting the first quadrant of the demagnetization curve to the full numerical solution minimizing the energy of a random collection of interacting unaxial magnetic particles in the presence of an applied magnetic field.

The energy function to be minimized is

$$E = \mu\ (H+\lambda M)\cos\phi - \mu H_a \cos^2(\phi-\theta),$$

where μ is the dipole moment, λ is the exchange constant for the mean field interaction, H is the applied field and H_a is the magnetic anisotropy field. The magnetization $M = \mu n\langle\cos\phi\rangle$ with n equal to the number of spins per unit volume, ϕ is the angle between the direction of magnetization and the applied field, and θ is the angle between the anisotropy axis of the particle and the applied magnetic field (Figure 1). For a random array of particles, the value of ϕ which minimizes E must be calculated for each particle in a self consistent manner.. For $\lambda = 0$, the problem reduces to the well known Stoner-Wolhfarth model. This approach has been effectively applied to a number of Rare Earth-Fe-B and Sm-Fe exchange-spring systems to determine both the interaction and the intrinsic properties of the grains as a function of both composition and temperature. The model also allows the accurate determination of the switching field distribution which determines the coercivity of the permanent magnet. Typical results are shown in Fig. 2.

Significance—The development of a powerful method of fully characterizing the magnetic properties of high energy product nanostructured permanent magnets, from measurement of a simple demagnetization curve, will allow the quantitative analysis of the role of chemistry and microstructure in both the intrinsic and extrinsic properties of these materials.

Contact: R. William McCallum, Ames Laboratory
Phone: (515) 294-4736, Fax: (515) 294-4291, E-mail: mccallum@ameslab.gov

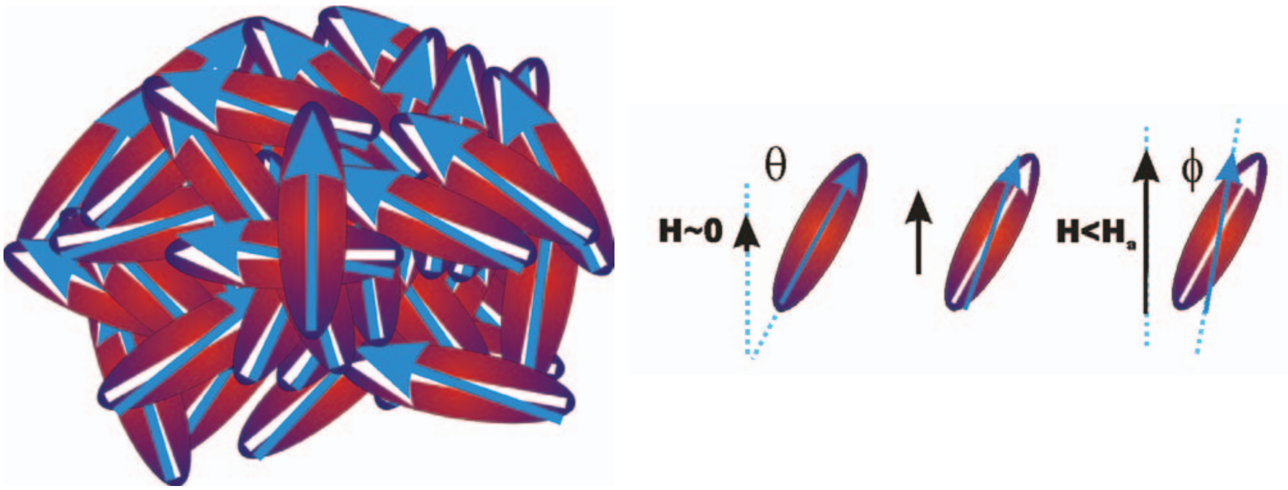

Figure 1. Random collection of uniaxial magnetic particles in an applied magnetic field and the direction of the magnetic moment of a particle as a function of the applied magnetic field.

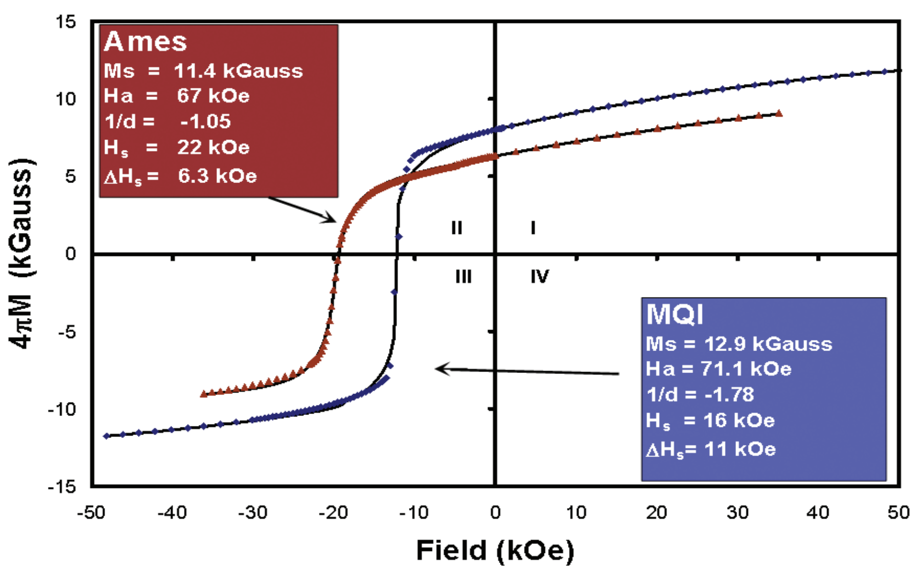

Figure 2. Model fits (solid lines) to the experimental room temperature demagnetization curves (dots) of two samples of $RE_2Fe_{14}B$ using the parameters determined from the 1^{st} quadrant fit and a normal distribution of switching fields. The Ames material (red) is designed for operation above 150°C while the Magnequench International (MQI) material (blue) is optimized for room temperature performance. H_s and ΔH_s are the mean and standard deviation of a normal distribution of switching fields. The interaction is given by a negative demagnetization factor $1/d \propto \lambda / H_a$.

Interparticle Dipolar Interactions in Magnetic Nanoparticle Assemblies

J. B. Kortright, *Lawrence Berkeley National Laboratory*
E. E. Fullerton *and* ***O. Hellwig[1],*** *Hitachi Global Storage Technology, San Jose Research Center*
S. Sun, *IBM Watson Research Center*

Motivation—Magnetic nanoparticles with a protective organic shell often self-assemble into densely packed arrays. In such arrays, close interparticle spacing increases the dipolar interaction energy between particles to compete with single-particle anisotropy, Zeeman, and thermal energies. While measurements of macroscopic magnetic properties have been interpreted in terms of interparticle dipolar interactions, it has remained challenging to measure their effects at the relevant interparticle dimensions. To fully understand the magnetic properties of these nanoparticle assemblies, and thereby assess their potential for technological applications, it is essential to measure the effects of dipolar interactions at these very short length scales.

Accomplishment—We developed resonant x-ray scattering techniques at LBNL's Advanced Light Source to obtain direct information about interparticle magnetic correlations in dense assemblies of 9-nm diameter Co particles of two different phases. Figure 1 shows scattering results for an assembly of particles having the ε-Co (cubic, low anisotropy) phase, and Figure 2 shows similar results for particles having *hcp*-Co (higher anisotropy) phase. In each case, the upper panels show the intensity *vs.* scattering vector q obtained at the Co L_3 absorption edge (778 eV) in zero and saturated applied fields. Each sample shows a peak at $q \cong 0.54\ nm^{-1}$, corresponding to strong interparticle interference. Subtle differences with magnetic field are shown in the intensity differences, ΔI_{lin} , in the lower panels. While a negative peak at the interparticle peak and positive feature at lower q are common features in each ΔI_{lin} , the relative intensity of the positive to negative features are very different for each sample. These differences can be interpreted in terms of the relative direction of the moments of neighboring particles, which in turn are influenced by dipolar interactions. Figure 3 shows how this information can be obtained by simulating the ΔI_{lin} , curve for the case of randomly oriented, uncorrelated moments. This model results in a ΔI_{lin} curve (Fig. 3b) having positive and negative features similar to those measured. This random orientation model accounts for the measured ΔI_{lin} for the *hcp*-Co assembly; thus we can distinguish no influence of dipolar interactions for this sample. However, for the ε-Co sample the positive intensity in ΔI_{lin}, is much stronger than that predicted for randomly oriented moments, implying that dipolar interactions having antiferromagnetic character are very strong in this sample.

Significance—These results demonstrate that dipolar interactions can, but do not necessarily, influence the average interparticle magnetic structure, even above the particles' blocking temperature when their moments are fluctuating due to the thermal energy. From these initial studies, it is clear that the particle anisotropy plays an important role in determining the extent to which interparticle dipolar interactions influence the magnetic structure. From a measurement perspective, these results demonstrate a new capability to resolve magnetic from chemical interparticle correlations. As such, they pave the way for future studies of magnetic interactions in similar nanoparticle assemblies that will evolve as our ability to tailor their material and geometric properties evolves.

Contact: Jeffrey B. Kortright, Lawrence Berkeley National Laboratory
Phone: (510) 486-5960, Fax: (510) 496-5530 E-mail: jbkortright@lbl.gov

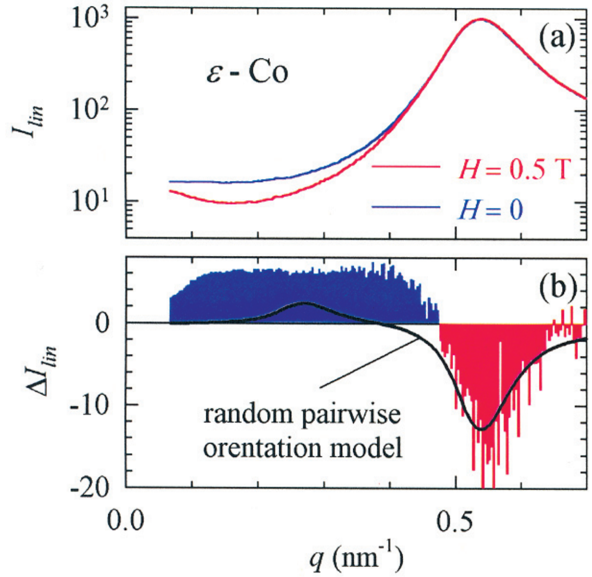

Figure 1. (a) Intensity of linearly polarized x-rays scattered from a dense assembly of ε-Co particles at remanence (blue) and in a near saturation applied field (red). (b) The difference $\Delta I = I(\mathrm{H} = 0) - I(\mathrm{H}_{sat})$ has negative (red) and positive (blue) features that are magnetic in origin. The black line is the predicted ΔI for randomly oriented, uncorrelated moments. This ε-Co assembly has much stronger intensity than the model at lower q, indicating preferred antiferromagnetic correlations resulting from dipolar interactions.

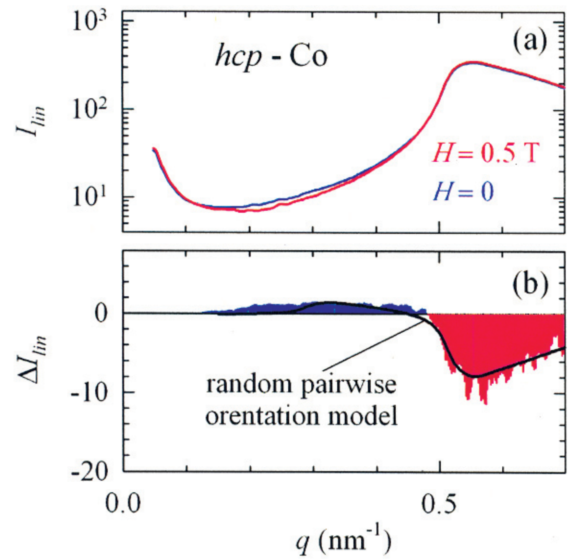

Figure 2. (a) Remanent and saturated q scans similar to those in Fig. 1a but for a dense assembly of *hcp*-Co particles. (b) For this sample the difference ΔI has positive (blue) and negative (red) features that are well described by the model for randomly oriented, uncorrelated moments on adjacent particles.

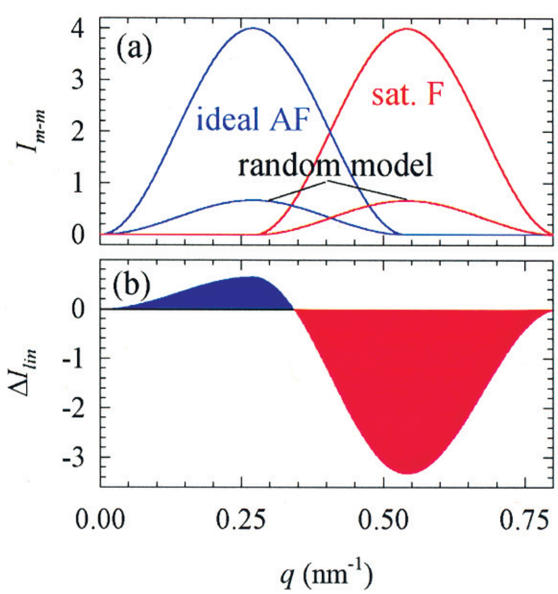

Figure 3. (a) Shows simulated magnetic intensity for structures in which all moments are saturated to have ferromagnetic (F) order, and an idealized antiferromagnetic (AF) order. If the moments are randomly oriented and uncorrelated, the structure has equal probability of F and AF order, and would scatter into both peaks with equal, reduced intensity. (b) shows the difference $\Delta I = I(\mathrm{H} = 0) - I(\mathrm{H}_{sat})$ calculated assuming that this random model describes the remanent (H = 0) state. The positive (blue) and negative (red) peaks have a distinct ratio for this random model. Dipolar interactions favoring a different remanent state will generally yield a different ΔI spectrum.

Local Chemistry Controls Stress-Induced Swelling in Polymers

Nitash P. Balsara *and* ***Hany B. Eitoun,*** *Lawrence Berkeley National Laboratory*
D. A. Loy, J. Stoddard, K. DeFriend, J. H. Small, *and* ***K. Wilson, Jr,*** *Los Alamos National Lab.*
L-Q Wang *and* ***Gregory J. Exarhos,*** *Pacific Northwest National Laboratory*
Chris Cornelius, *Sandia National Laboratories, NM*
K. J. Shea, *SUC Irvine*
Alexander DeQuan Li, *Washington State University*

Motivation—Polymers that exhibit reversible volume changes upon exposure to heat, light, chemical environment, or applied potential are enabling materials for many applications including molecular valves, drug immobilization templates within the body, self-repairing structures, and many others. To achieve this desired response requires modifying the chemical structure of a polymer to incorporate chromophore or electroactive moieties that respond to incident light or an applied electrostatic potential. Alternatively, the presence of electronegative chemical groups that undergo hydrogen bonding interactions with an ambient solvent or the polymer itself can lead to temperature or solvent-dependent changes in volume. Incorporation of the appropriate chemical groups in the polymer chain and understanding how they influence chain conformation and packing are critical to the development of polymeric materials that reversibly swell and contract in response to changes in local environment.

Accomplishment—Innovative approaches to synthesizing copolymers that exhibit reversible volume changes when subjected to an applied stimulus have been developed. Figure 1 shows an organometallic block copolymer that transforms from an ordered lamellar phase to a disordered, higher volume phase when the oxidation state of the resident iron atom in the attendant ferrocene complex is changed, either by addition of a chemical agent to the accompanying solution or by application of a weak electric field. The volume change associated with this order-disorder transformation is reversible upon reduction of the block copolymer. In related work, a copolymer containing a chromophore bridging group (Fig. 2) suffers cleavage upon irradiation with short wavelength light leading to a higher volume state. Irradiation of the expanded copolymer at longer wavelengths repairs the broken bond thereby leading to a decrease in polymer free volume. The final example concerns a sulfide-functionalized hydrogel that binds to gold nanoparticles (Fig. 3). Near room temperature, resident hydrogen bonding maintains the composite in an expanded state where the gold particles are separated and the composite appears clear. At slightly elevated temperatures, the weak hydrogen bonds break and the hydrogel collapses thereby coalescing the gold particles and rendering the composite opaque.

Significance—Passive control of polymer free volume has been achieved in three functionalized polymer systems that respond reversibly to heat, light, applied electric field, or solution chemistry. Understanding the transformation dynamics of such systems underpins development of functionalized polymer systems that act as valves to control molecular diffusion, as smart matrices for release of therapeutic agents, or as optical limiters for communications or related optical shutter applications.

Contact: Gregory J. Exarhos, Pacific Northwest National Laboratory
Phone: (509) 376-4125, Fax: (509) 376-5106, E-mail: greg.exarhos@pnl.gov

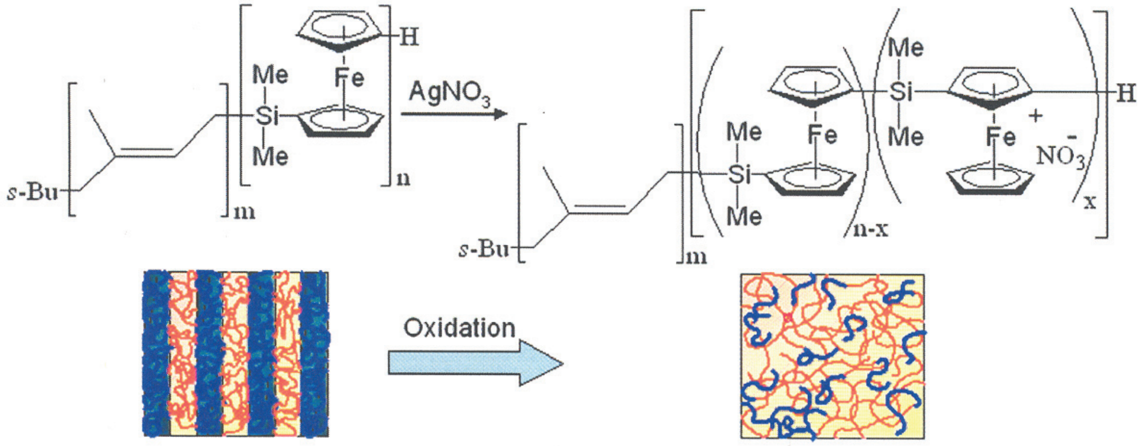

Figure 1. Ferrocene to ferrocinium cation transformation that induces polymer disorder is driven by an applied external field (2 V/cm) or by addition of an oxidizing agent (Ag^{+1}).

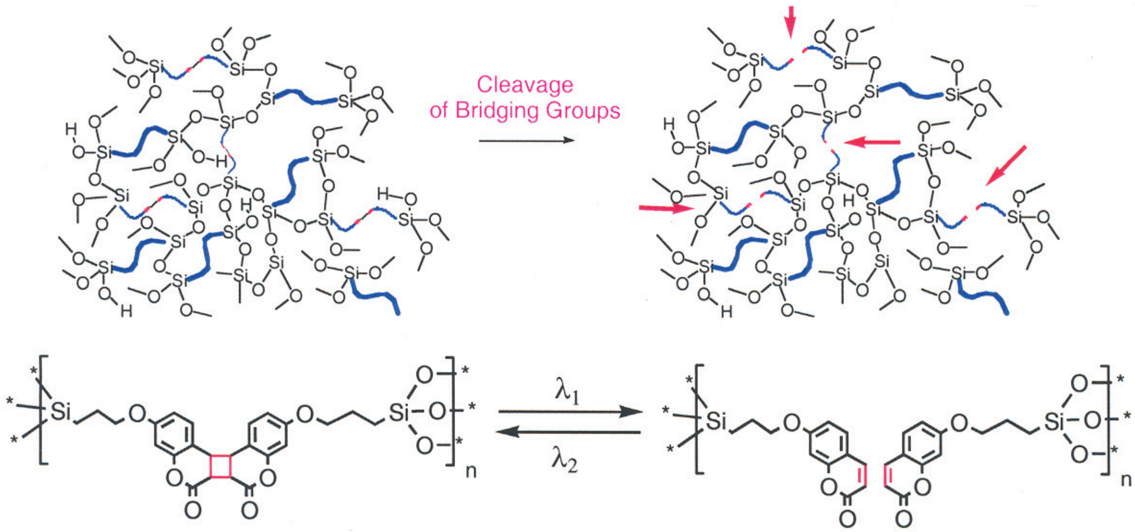

Figure 2. Short wavelength light (λ_1) cleaves the coumarin-dimer weak link and swells the polymer. Longer wavelength light (λ_2) reestablishes the link, and shrinks the polymer.

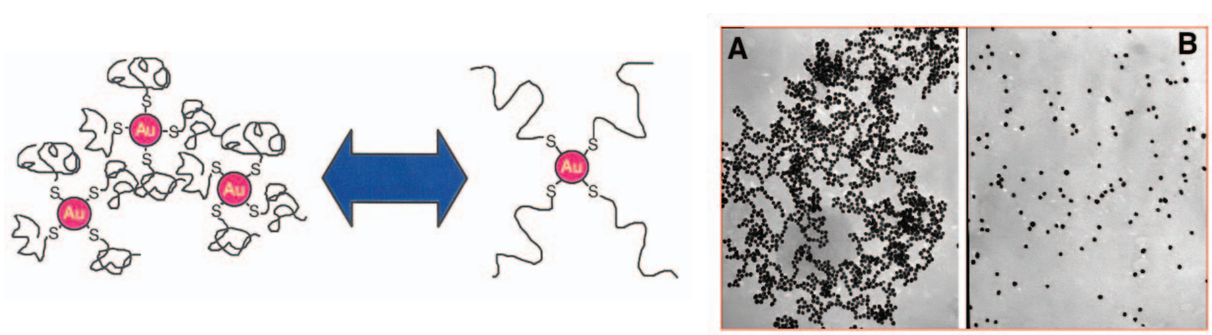

Figure 3. A gold functionalized hydrogel solution transforms to an opaque (A), low volume state above a critical temperature but becomes clear (B) as the temperature is lowered and the hydrogel expands. (12 nm diameter gold nanoparticles are seen in the micrograph).

Hydrophilic Polymer Templates for Molecular Sequestration and Release

P. V. Braun, Y.-J. Le, *and* ***A. Pruzinsky,*** *University of Illinois, MRL*
B. C. Bunker *and* ***D. L. Huber,*** *Sandia National Laboratories, NM*

Motivation—Understanding the mechanism by which large molecules bind to polymer surfaces is critical for developing substrates that can be reversibly switched from an absorption state to a desorption state. The volume change exhibited by hydrogels upon heating or as a function of solution ionicity can be exploited to develop templates that not only can signal the presence and concentration of a targeted analyte, but also can be used to either trap molecules from or add molecules to solution.

Accomplishment—The specific volume of a polymer hydrogel in contact with an aqueous solution is dependent upon local temperature, solution pH, and solution ion content making it an ideal candidate material for both sensing and binding target molecules. In one study, a vinyl functionalized phenylboronic acid is copolymerized with a hydrogel. The modified block copolymer now is able to trap glucose in an ionic complex leading to a swelling of the polymer. Binding of glucose to this support is a dynamic process and dependent upon its concentration in solution. When the hydrogel is fabricated into an ordered hcp array using colloidal templating techniques, a photonic crystal results that will change its lattice spacing when the polymer swells in response to the presence of glucose. Bragg diffraction of light from the array is dependent upon lattice spacing (Fig. 1) and will shift in wavelength as the lattice changes size. The magnitude of the change in lattice constant is related to the amount of glucose in solution. In related work the compaction of a hydrogel, a modified (poly-n-isopropyl acrylamide) - PNIPAM - in an aqueous solution at temperatures near 50°C can be used to trap large protein molecules. Upon lowering the temperature, the gel swells thereby releasing the protein into solution. Fig 2 shows the schematic of an electrokinetic pumping experiment where a dilute solution of a fluorescent-tagged myoglobin is passed through a modified PNIPAM plug in a capillary column. Protein capture and release is confirmed from fluorescence emission data of the free protein as it releases from the column upon lowering the temperature. A high efficiency for reversible protein binding has been demonstrated. New polymer formulations have been developed that allow the polymer to be used directly in the column without the addition of a solid support medium.

Significance—Hydrogel based materials that exhibit reversible volume changes in a physiological temperature range can be used in biological applications that include real-time sensing of large molecules dissolved in solution and controlled release or sequestration of proteins. Real-time measurement of sugar in blood is but one application that demands follow-on research. Other applications are focused on using these materials in studies of the human immune system and as a means for sequestering of and early detection of pathogens.

Contact: P. V. Braun, University of Illinois/F5-MRL
Phone: (217) 244-7293, Fax: (217) 333-2736, E-mail: pbraun@uiuc.edu

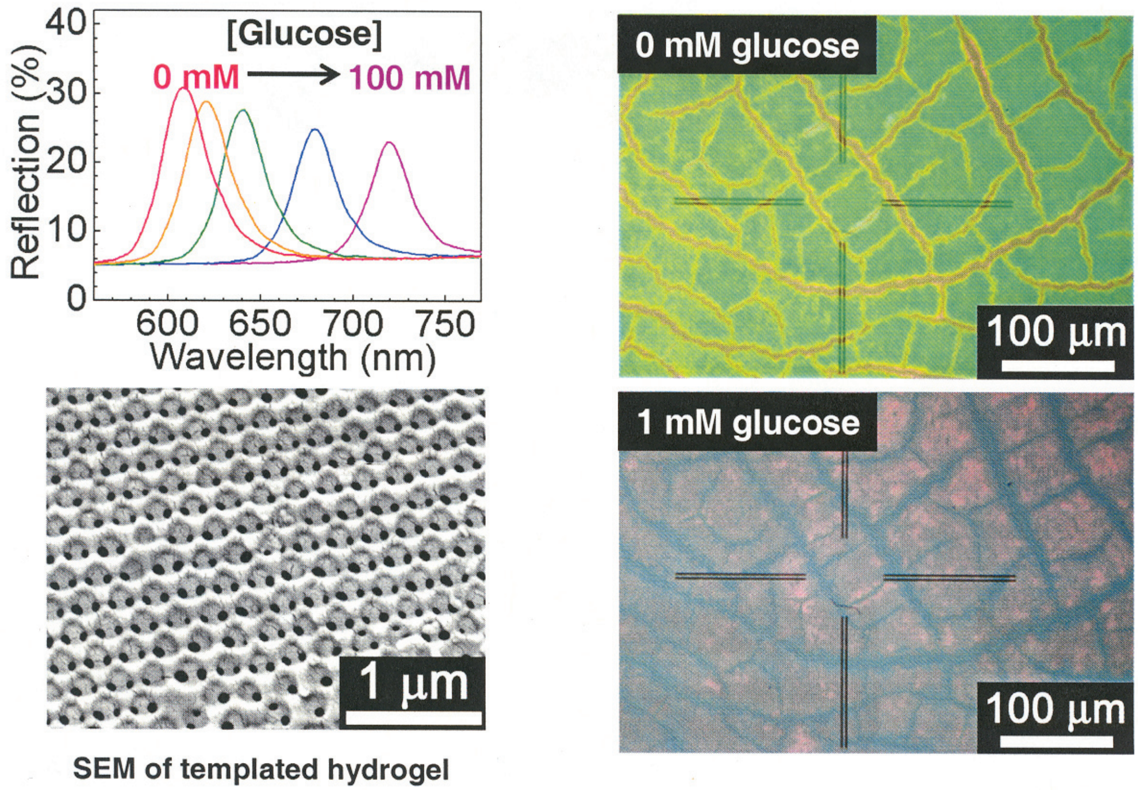

Figure 1. A periodic hydrogel array reversibly swells when glucose binds to the surface yielding a change in color (reflection spectrum - top left). As the hydrogel swells, the diffracted light is red shifted allowing the glucose concentration to be quantified. Images on the right show the swelling.

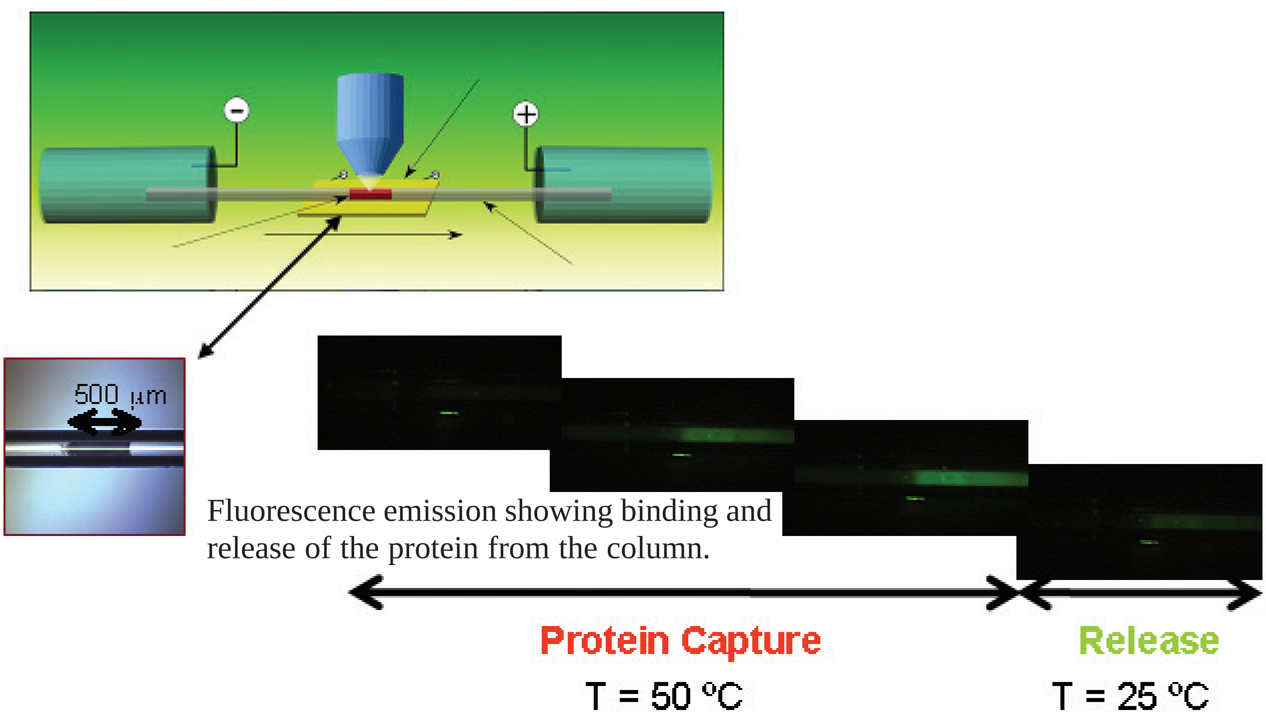

Figure 2. A modified capillary column containing the hydrogel, poly(n-isopropyl acrylamide) shows high efficiency for protein capture and release as the column temperature cycles between 50°C and 25°C.

Molecular Self-Assembly and Ordering in Block Copolymers and Blends

Surya Mallapragad, *Ames Laboratory*
Hau Wang, *Argonne National Laboratory*
A. Habenschuss *and* ***M.-H. Kim,*** *Oak Ridge National Laboratory*
J. G. Curro *and* ***D. R. Heine,*** *Sandia National Laboratories, NM*

Motivation—Self-assembly, that drives structural evolution of copolymers and ordering phenomena in polymer blends, is controlled by both inter- and intra-molecular interactions among the resident hydrophilic and hydrophobic regions that comprise the polymer chains, their respective number density, and size. Parameterized models that simulate these interactions and subsequently predict stable arrangements (lamellar, gyroid, core-shell cylinder structures) have been developed and continue to improve. The ability to both design multi-component block copolymer systems with integrated chemical functionality and predict the stable structures that will result is key to developing complex systems that spontaneously order under the influence of temperature, solution polarity, and pH.

Accomplishment—Observed ordering phenomena in soluble block copolymer systems are strongly influenced by interactions with the attendant solvent. Solvent polarity and pH are two critical solution parameters that influence hydrogen-bonding interactions which in turn direct formation of ordered polymer structures. The type of structure that results also depends upon the nature and size of contrasting chemical regions (polar and non-polar) that comprise the polymers. In recent studies of oligo(phenelenevinylene)-poly(ethylene-glycol) based diblock copolymers (OPV-PEG) the length of the glycol linkage (ethylene or propylene) was found to affect polymer chain ordering in solution. Three distinct regions were found in tetrahydrofuran (THF)/water solutions as the water content of the solution, and hence, hydrogen bonding capacity of the solution, increased. Solutions in excess of 14% water directed formation of ordered fiber bundles that could be imaged by their photoluminescence when irradiated with 400 nm light. (Fig. 1) In related work, more complex pentablock copolymers comprised of poly (ethylene- and propylene oxide) blocks and an alkylamino-ethylmethacrylate block undergo self-assembly to form micelles which in turn further interact to form ordered nanoscale micellular composites. Self-assembly and dis-assembly was found to be controlled by both solution pH and temperature and was seen to occur over multiple length scales. (Fig. 2)

Significance—Enhanced solution hydrophilicity directs block copolymer nanofibers to self align and subsequently assemble into fiber bundles. Such bundles exhibit waveguiding properties and can be induced to photoluminesce upon excitation at short wavelengths. Methods to promote self-assembly across multiple length scales is paramount to continued development of a bottoms-up approach to synthesize complex structures from simple building blocks. The demonstration of micelle self-assembly across multiple length scales also is critical to develop next-generation hierarchical approaches to generating complex structures. Understanding the weak polymer chain interactions that control the ordering process is paramount to this end.

Contact: Hau Wang, Argonne National Laboratory
Phone: (630) 252-3461, Fax: (630) 252-9151, E-mail: hau.wang@anl.gov

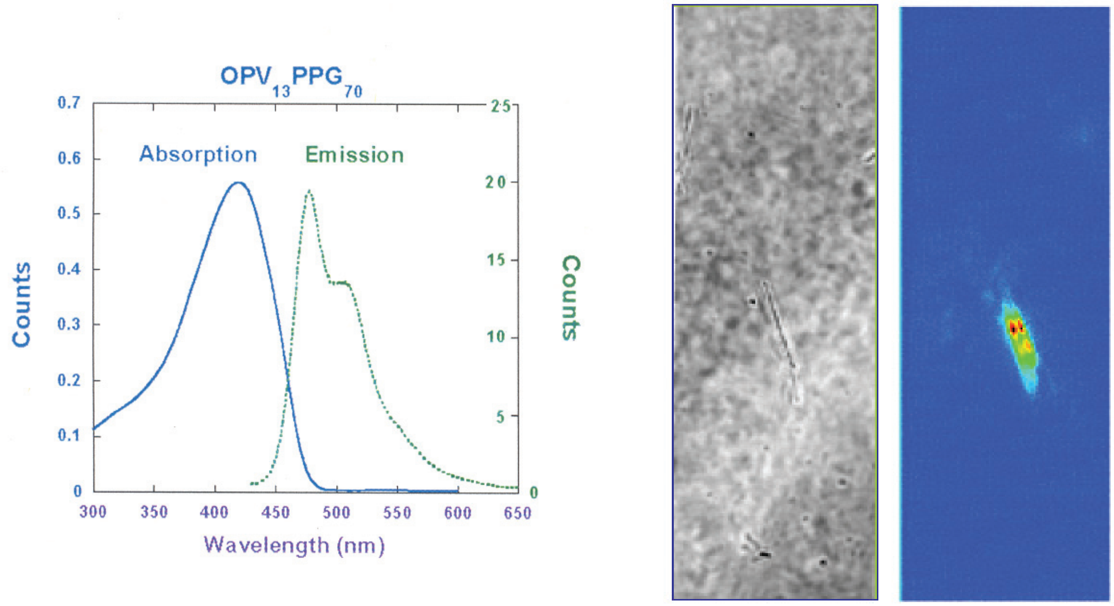

Figure 1. Absorption and emission spectra from the phenylvinylene blocks within the copolymer. The bright light image (gray) and photoluminescence image (blue) are shown at the right and reveal images of the fiber bundles. (Image size: 32mm x 102mm).

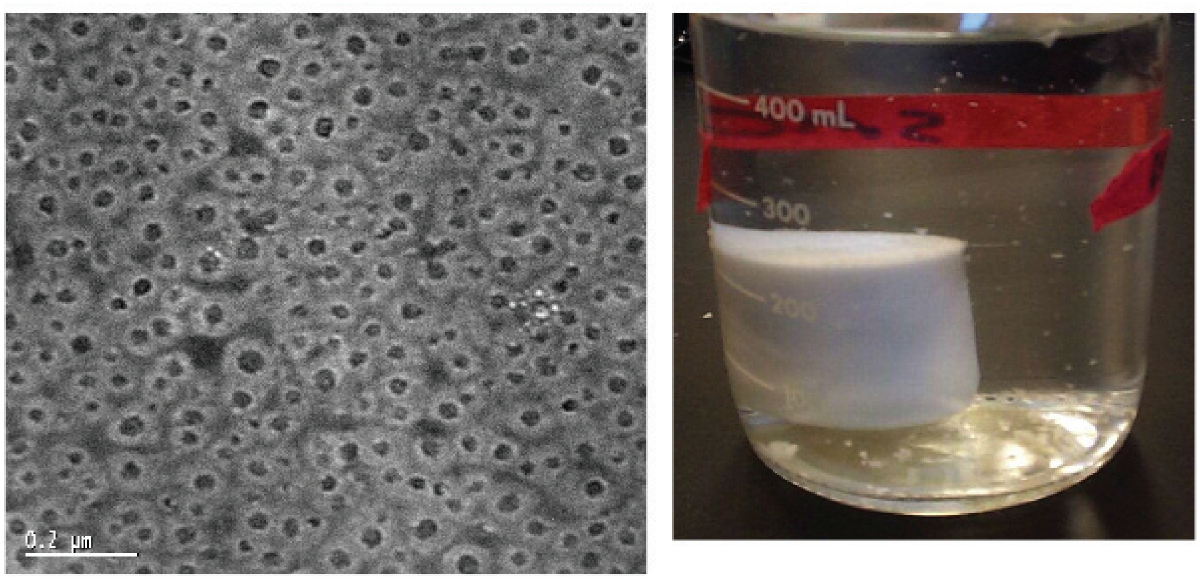

Figure 2. Cryo-TEM image of pentablock copolymer micelles (left) and the self assembly of these micelles into a macroscale solid at high pH (right). At low pH, the polymer hydrogel is soluble due to electrostatic repulsion between charged regions on the polymer chains.

Nanoscale Science of Novel Amorphous $Ti_xAl_{1-x}O_y$ High Dielectric Constant Films

O. Auciello, W. Fan, *and* ***B. Kabius,*** *Argonne National Laboratory*
C. Lopez *and* ***E. A. Irene,*** *University of North Carolina - Chapel Hill*

Motivation—High dielectric constant (*k*) metal oxides are being considered as alternative gates to SiO_2 to provide a substantially thicker (physical thickness) dielectric layer with low leakage and density of trapping states and sufficiently high gate capacitance. However, substantial fundamental science is needed to develop the next generation of nanoscale high-*k* dielectric CMOS gates. Efforts are directed to finding reliable high *k* oxides with high capacitance and all critical properties required for CMOS gates. A trade-off between dielectric constant and band-offset height is generally observed on gate oxides.

Accomplishment—Combining TiO_2 and Al_2O_3, with the two extremes of high *k* and high band offset, we produced a novel alloyed oxide ($Ti_xAl_{1-x}O_y$) or TAO, with high and low tunneling leakage. We developed a room temperature oxidation process to produce ultra-thin TAO layers on Si with sub-atomic or no SiO_x interface formation, via exposure to atomic oxygen, subsequent to sputter-deposition of a metallic TiAl alloy. We demonstrated TAO layers with < 0.5 nm equivalent oxide thickness, *k* = 28-30, and leakage 10^4-10^5 orders of magnitude lower than that of equivalent SiO_2 layer. We obtained insights into fundamental physics and materials science of the new layer.

The specific composition of TiAl = 75:25 at % was chosen for the synthesis of the TAO dielectric layers investigated in this initial work. It was expected, from thermodynamic and kinetic considerations of alloy formation that by introducing a moderate amount of Al_2O_3 into the TiO_2 matrix, both the leakage performance and thermal stability of TiO_2 could be improved without sacrificing much of its high permittivity. *In situ* XPS analysis on the TiAl thin layers immediately after oxidation, revealed that the complete transitions of Ti^0 to Ti^{4+} and Al^0 to Al^{3+} occurred within the entire temperature range (25 to 700 °C). Indistinguishable XPS spectra for Ti^{4+} and Al^{3+} were observed on all TAO layers, suggesting formation of stoichiometric alloy oxides with identical chemical bonding produced by oxidation in atomic oxygen at high temperature as well as room temperature (r.t.).

TEM study on the r.t. oxidized TAO thin layers revealed two amorphous layers as seen in Fig. 1, a darker top layer (L2) with a thickness of about 3 to 4 nm and a brighter intermediate layer (L1) with a width of <2 nm. Elemental analysis revealed that L2 contains a higher concentration of Ti and that L1 is enriched in Al. *C-V* measurements of dielectric layers grown on n^- Si showed very high capacitance densities of 7.7 - 8.3 µF/cm^2 (Fig 2).

Significance—The Al results on the novel amorphous TAO layer provided unique insights into oxidation process in alloys. In addition, the novel alloyed oxides ($Ti_xAl_{1-x}O_y$) appear to be potential candidate materials for a new generation of high *k* dielectric gates for metal/oxide /semiconductor structures.

Contact: Orlando Auciello, Argonne National Laboratory
Phone: (630) 252-1685, Fax: (630) 252-4289, E-mail: auciello@anl.gov

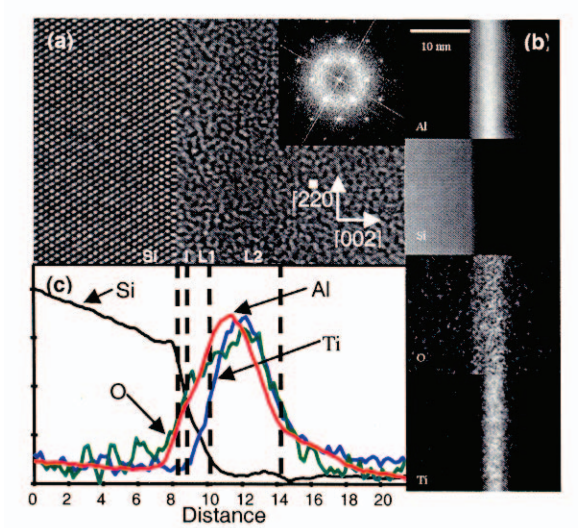

Figure 1. HRTEM and EELS analyses of room-temperature oxidized TAO layer grown on Si(100). (a) HRTEM image, (b) elemental maps and (c) integrated line scans for Al, Si, O and Ti, respectively.

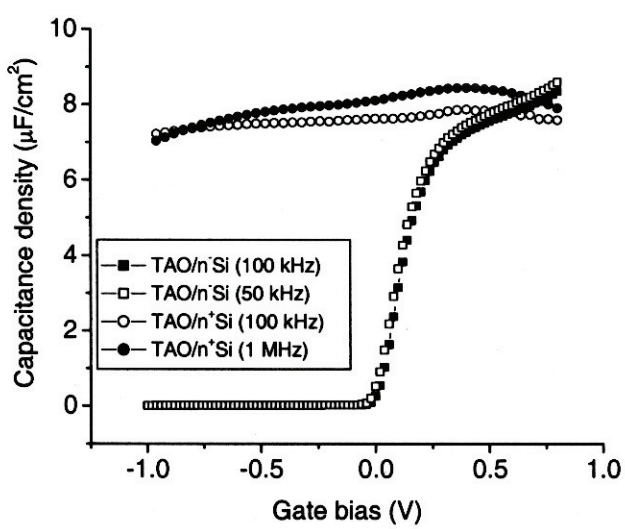

Figure 2. *C-V* characteristics of the TAO-based MOS capacitors on n$^-$ and n$^+$ Si, measured at different frequencies. Very high accumulation capacitance densities (7.7 - 8.3 μF/cm^2), corresponding to an equivalent oxide thickness less than 0.5 nm, were achieved on different types of Si substrates with the RT oxidation technique developed in this study.

Complex Dynamical Behavior in Ferroelectric $LiNbO_3$

S. R. Phillpot, *Argonne National Laboratory and University of Florida*
V. Gopalan, *Pennsylvania State University*

Motivation—Ferroelectric lithium niobate ($LiNbO_3$) has emerged as an important materials in surface acoustic wave (SAW) devices and in nonlinear optical applications such as electro-optics and second-harmonic generation. Despite these wide-ranging applications, much remains to be understood as regards the fundamental physics and materials science of $LiNbO_3$.

$LiNbO_3$ is trigonal with an $R\bar{3}c$ structure in the paraelectric phase. With the onset of ferroelectricity at T_c~1210 °C (1483K), the crystal structure remains trigonal, but the inversion symmetry of the system is lifted, reducing the system to the R3c structure. The objective of this work was to use molecular-dynamics (MD) simulations to probe the dynamical response of ferroelectric $LiNbO_3$.

Accomplishment—The key measure of a ferroelectric material is its polarization. The MD simulations showed that while below ~500K the polarization in $LiNbO_3$ decreases only rather weakly with temperature, above 500K it drops off essentially linearly with temperature up to a Curie temperature of T_c~1400K. This simulated value of T_c was in pleasingly good agreement with the experimental values of 1483K. To characterize the ferroelectric-paraelectric phase transition and its dynamics, we probed the two key structural differences between the ferroelectric and paraelectric phase: namely the positions of.the Li ions with respect to their associated oxygen planes and the displacement of Nb ions from the centers of their oxygen cages.

We found the dynamical responses of the Li-O planes and Nb-O cages to be very different. As expected, in the ferroelectric phase the Li ions were found to all be displaced either above or below their associated O planes. However, even in the paraelectric phase, the Li ions were displaced out of the plane of oxygen ions in which, crystallographically. they would be expected to lie. This is characteristic of order-disorder dynamical behavior.

The Nb ions were found to be displaced from the centers of their associated oxygen cages at low temperatures, but sat at the crystallographically expected positions at the center of the cages at higher temperatures. This is characteristic of displacive dynamics. Moreover, it as found that this ferroelectric behavior in the NbO_6 cages disappeared at ~900K, i.e., ~500K below T_c. We thus concluded that between 900K and 1400K the ferroelectric response of the material is supported on by the Li-O planes.

Significance—$LiNbO_3$ has been shown to display an unusual dynamical response with both order-disorder and displacive dynamics. Moreover, the transition temperatures for the two distinct contributors to the ferroelectric response were found to be very different from each other.

Contact: Simon R. Phillpot, University of Florida
Phone: (352) 846-3782, Fax: (352) 846-3355, E-mail: sphil@mse.ufl.edu

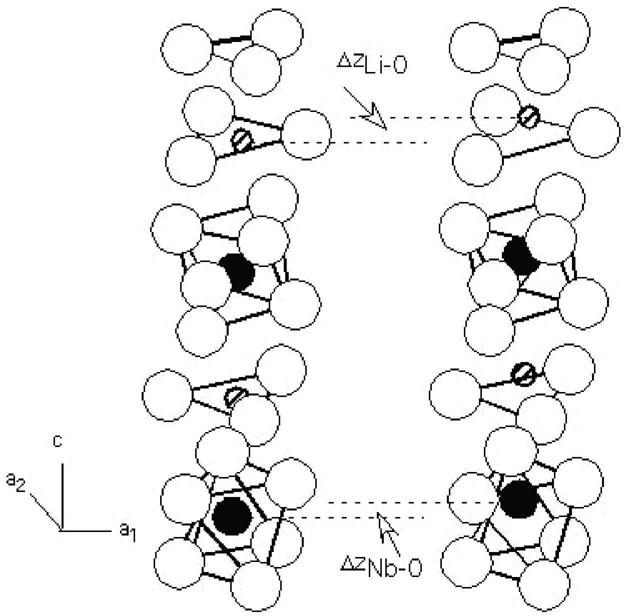

Figure 1. Schematic of the paraelectric (left) and ferroelectric (right) phases of $LiNbO_3$. The ferroelectric distortions associated with the displacement of the Nb ions (solid circles) from the center of the octahedral cages of oxygen ions (open circles) is $\Delta_{zNb\text{-}O}$. The displacement of the Li ions (shaded circles) from the associated planes of oxygen ions is $\Delta_{zLi\text{-}O}$.

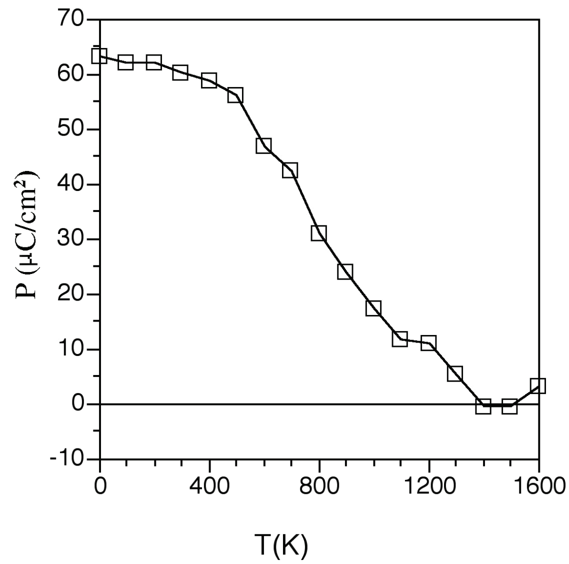

Figure 2. Calculated temperature dependence of the polarization. The linear decrease in the polarization with temperature above 500K extrapolates to a T_c~1400K, which is consistent with the experimental value of T_c=1483K. The small non-zero values of the polarization above T_c are an artifact of the finite system size, and decrease in magnitude for larger systems and longer simulation times.

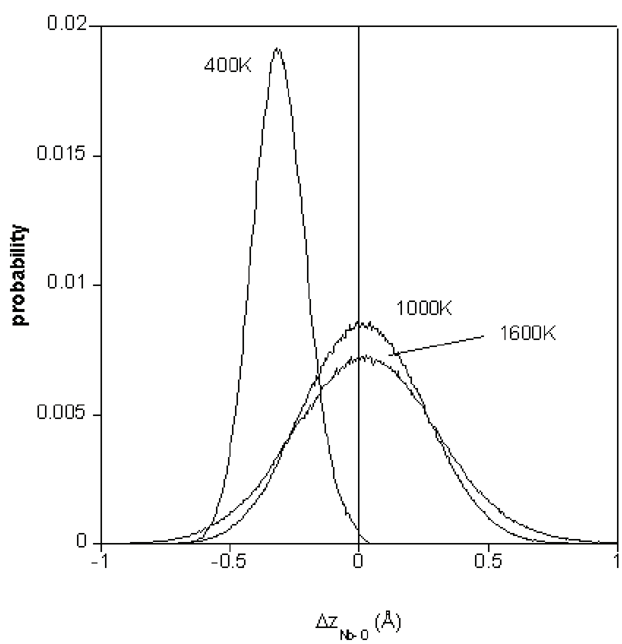

Figure 3. The probability distribution functions for the displacement of a Nb ion from the center of the O cage, $\Delta_{zNb\text{-}O}$, is unimodal at 400K, characteristic of the ferroelectric phase. The unimodal distributions centered at zero displacement at both 1000K and 1600K are characteristic of a paraelectric system undergoing displacive dynamics.

Dielectric Response in $KTaO_3/KNbO_3$ Superlattices

D. P. Norton, *University of Florida*
L. B. Boatner, *Oak Ridge National Laboratory*

Motivation—In insulating materials, the bonding of atoms is the result of electron exchange from cations to anions. This valence electron exchange creates a distribution of separated charges (dipoles) whose mutual interactions dictate the properties of the material. If these dipoles spontaneously align parallel with one another, this is called ferroelectricity. Using an electric field, the alignment of the dipoles can be switched, yielding so-called ferroelectric memory devices. Antiparallel alignment of dipoles in adjoining unit cells leads to antiferroelectricity. It is the atom-to-atom interactions that determine the overall dielectric response of a material. An interesting fundamental question is whether the dipole ordering phenomenon is different for nanoscale dielectrics as compared to bulk materials. Recent advances in oxide film growth, particularly for dielectric perovskites, have enabled the use of nanoscale superlattices and heterostructures for investigating intrinsic and extrinsic size effects on dipole ordering. As a result of superlattice formation, radical changes in the ferroelectric response can be realized.

Accomplishment—The effects of finite size on ferroelectric ordering has been examined for a specific ferroelectric material system, namely $KNbO_3$. In particular, $KNbO_3/KTaO_3$ superlattices, schematically shown in Figure 1, have been grown as crystalline thin-film structures. $KTaO_3$ has the same crystal structure as $KNbO_3$, but is paraelectric. The dipole ordering behavior of these structures can be experimentally examined by measuring the dielectric constant through devices known as interdigitated capacitors. The capacitance is directly proportional to the dielectric constant. The properties of $KNbO_3/KTaO_3$ superlattices were measured in which the thickness of the $KNbO_3$ layer was only a single unit cell. The question being addressed is, "does the dipole ordering fundamentally change when the thickness of the bulk ferroelectric is reduced to only a few atoms thick?" The expectation is that the reduction in thickness will either have no effect or simply impeded the dipole ordering as seen in ferroelectric materials. Experimentally, an unexpected result was observed. The dielectric response of the superlattice does not coincide with either the ferroelectric or paraelectric phase. Instead, it is consistent with *antiferroelectric ordering* as illustrated in Figure 2. Since neither $KTaO_3$ nor $KNbO_3$ exhibits antiferroelectricity, the response appears to be a result of the artificial B-site ordering created in the superlattice structure.

Significance—This study of $KNbO_3/KTaO_3$ superlattices indicates that dipole ordering behavior in ferroelectric materials is significantly modified by a reduction in size. Fundamentally, the anti-parallel ordering needs to be theoretically explained. For applications involving ferroelectric/paraelectric materials for memory or tunable microwave electronics, these results indicate a fundamental limitation when dealing with very thin layers.

Contact: David Norton, University of Florida
Phone: (352) 846-0525, Fax: (352) 846-1182, E-mail: dnort@mse.ufl.edu

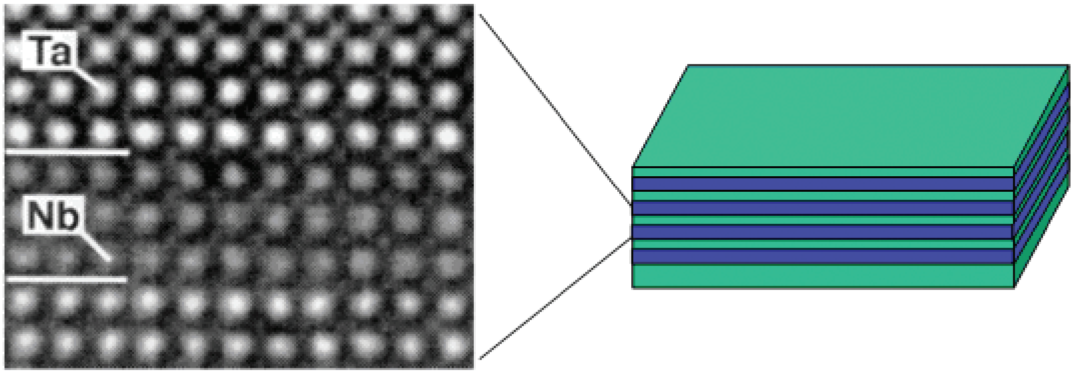

Figure 1. $KTaO_3/KNbO_3$ superlattice structures were used to understand the effects of reduced size on dipole ordering in ferroelectrics. The high-resolution scanning transmission electron microscopy image was provides by Matthew Chisholm at ORNL.

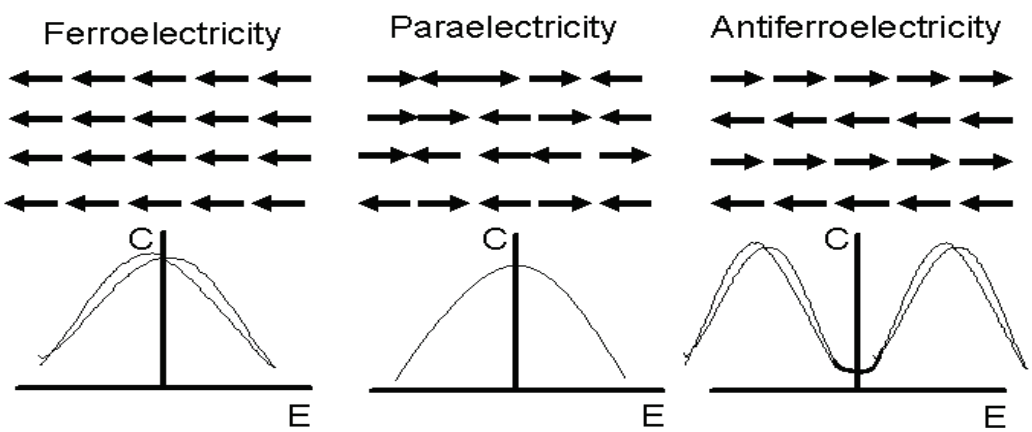

Figure 2. From the capacitance response of the superlattice structures, dielectric behavior consistent with antiferroelectricity is observed. This is contrary to what is seen in bulk materials and indicates the effects of reduced dimensionality. C = capacitance, E = electric field.

Novel Multifunctional Carbon Nanofiber Scanning Probe Tips

Hongtao Cui *and* ***Douglas H. Lowndes,*** *Oak Ridge National Laboratory*

Motivation—The tip is a key part of a scanning probe microscope and a variety of probe tips have been developed. Although high-aspect ratio and sharp probe tips made of silicon are commercially available, they are somewhat expensive and not sufficiently robust to survive "tip-crash" with the surface during microscope operation. Cylindrical carbon nanotubes (CNTs) also have been used as probe tips due to their high aspect ratio and nanometer-sized diameter. However, all fabrication processes experience difficulties in controlling the number of CNTs on a cantilever as well as their lengths and orientations, which are critical to control image quality. When used in magnetic force microscopy (MFM), probe tips can be made of magnetic wires, or commercial scanning probe tips are coated with magnetic thin-film materials. But tremendous effort is needed to optimize those tips and acquire quantitative data. For biological applications, probe tips may need to be chemically functionalized in order to image functional groups on the surface of DNA or other bio-molecules. Carbon nanofibers (CNFs) are quite robust and have a large aspect ratio with tip diameters in the range of a few tens of nanometers, which makes them suitable for scanning probe applications. CNFs have a tip-growth mode, in which a Ni or Fe catalyst nanoparticle is located at the tip of the growing CNF. Their magnetic nature makes such CNFs promising as probe tips for MFM. CNFs also can be functionalized *in situ*, and thus can be used to probe the surface of biological samples. The mechanical and chemical properties and functionalities of CNF probe tips can be further varied by depositing novel materials, e.g. nanodiamond.

Accomplishment—Figure 1 shows different SEM views of CNFs grown on tipless cantilevers, with the images taken at different angles and magnifications. Fig. 1(a) shows that a CNF is only grown where a catalyst particle is located, and only one CNF is nucleated there if the initial evaporated catalyst "dot" has suitably small diameter and thickness (e.g. 200 nm diam x 20 nm thick). The CNF has a length of 3.1 µm. Figs. 1(b-d) show front views of the CNF, revealing that it is almost perpendicular to the cantilever beam surface. However, the side views in Figs. 1(e-g) show that the CNF is tilted away from the cantilever surface normal. The tilt angle ranges from 15° to 18°. The catalyst nanoparticle can be seen at the tip of the CNF, and its shape directly defines the probe tip. The CNF has a conical shape, with its diameter gradually reducing from base to tip. The conical shape can be controlled, for example, by varying the C_2H_2 flow rate, as is seen by comparing Fig. 1(e) with Fig. 1(h). It is clearly seen that CNFs transform from cylinder-like (Fig. 1(h)) to cone-like (Fig. 1(e)) with an increase of the acetylene flow rate from 56 sccm to 59 sccm. The full tip angle of the conical CNFs can be controlled up to 8.5°. Figs. 1(i) and 1(j) show a front view and a side view, respectively, of a CNF grown using an iron catalyst particle. The large catalyst particle has a non-symmetrical shape and clearly defines the tip geometry. Figs. 2(a) and 2(b) show the topographic and magnetic force gradient images, respectively, of a magnetic tape that were obtained using the CNF probe.

Significance—CNFs can be grown with their length, shape, aspect ratio, tip sharpness, and tip magnetism reasonably well controlled. They also provide a medium for nucleation/growth of other novel materials to enhance mechanical, electronic, and chemical functionalities.

Contact: D. H. Lowndes, Oak Ridge National Laboratory
Phone: (865) 574-6306, Fax: (865) 576-3676, E-mail: lowndesdh@ornl.gov

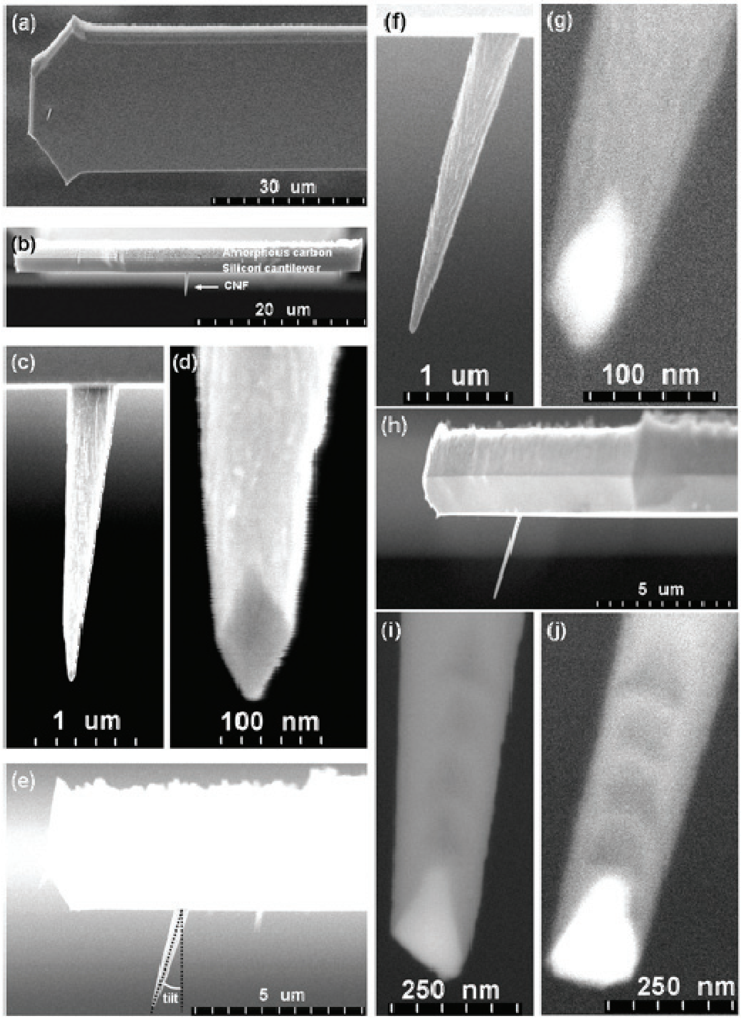

Figure 1. SEM images of CNFs taken at different angles: (a) side view of a CNF with 45° tilt; (b), (c), (d) front views of the CNF at different magnifications; (e), (f), (g) side views at different magnifications; (h) side view of a different CNF; (i) and (j) front view and side view of a CNF nucleated using a large iron catalyst particle.

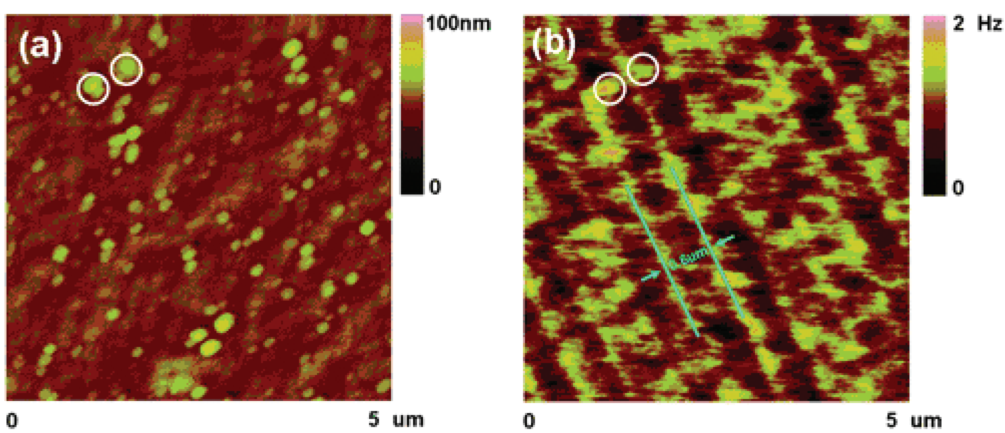

Figure 2. (a) Topographic image of a magnetic tape; (b) the corresponding magnetic force-gradient image, revealing a surface with large protrusions and longitudinal magnetic tracks with ~0.6 µm peak separation. Note that surface roughness has a strong additional influence in the magnetic force image, since topographic features appear also in the magnetic force image (e.g., see the features highlighted with circles).

Synthesis of a Self Assembled Hybrid of Ultrananocrystalline Diamond and Carbon Nanotubes

Xingcheng Xiao, Jeffery W. Elam, Susana Trasobares, Orlando Auciello, *and* ***John A. Carlisle,*** *Argonne National Laboratory*

Motivation—Recent strong scientific and technological interest in nanostructured carbon materials (nanocarbons) is motivated by the diverse range of physical properties these systems exhibit. Among them, carbon nanotubes (CNTs) and nanocrystalline diamond (NCD) are attracting most attention due to their respective unique properties. The synergistic combination of CNTs and NCD could give rise to materials with novel properties that could be used advantageously in applications such as electronic devices or MEMS/NEMS. However, the reported conditions for growing CNTs and NCD are different from each other, which make the preparation of nanocomposite based on CNTs and NCD complicated. A synthesis pathway must be developed that would lead to the concurrent growth of different allotropes of carbon that are covalently bonded and organized at the nanoscale.

Accomplishment—We demonstrated for the first time that the simultaneous synthesis of ultra-nanocrystalline diamond (UNCD) and CNTs can be achieved to form a covalently bonded hybrid material: a nanocomposite of diamond and CNTs. Through controlling the initial nucleation condition for UNCD and CNTs by selectively addressing nanodiamond seeds and transition metal catalyst, the relative fraction, morphology of UNCD and CNTs have been controlled correspondingly (Fig. 1). Multiwalled CNTs have been successfully prepared with hydrogen-poor carbon-containing plasma of 99%Ar/1%CH_4 (Fig. 2). Single-wall CNTs (SWCNT) could be also integrated into the film, as evidenced by radical breathing mode (RBM) peaks (Figure. 3). This result combined with other results has led to a fundamental re-evaluation of the growth processes that occur during the growth of UNCD thin films, and also demonstrated a new synthesis pathway for making materials that combine allotropes of carbon at the nanoscale.

Significance—The growth process established in the research on synthesizing the allotrope nanocarbon may provide a methodology for synthesizing nanostructured materials. The method offers a novel approach to modulate the relative ratio of sp^2- and sp^3-bonded carbon to form self-assembled carbon nanostructures. These structures should be amendable to modern patterning techniques to further organize them for the development of more efficient, high temperature field electron and thermionic emitters, novel nanoelectronics, MEMS/NEMS, and self-lubricant protective coatings.

Contact: J. A. Carlisle, Argonne National Laboratory
Phone: (630)-252-9555, Fax: (630)-252-3520, E-mail: carlisle@anl.gov

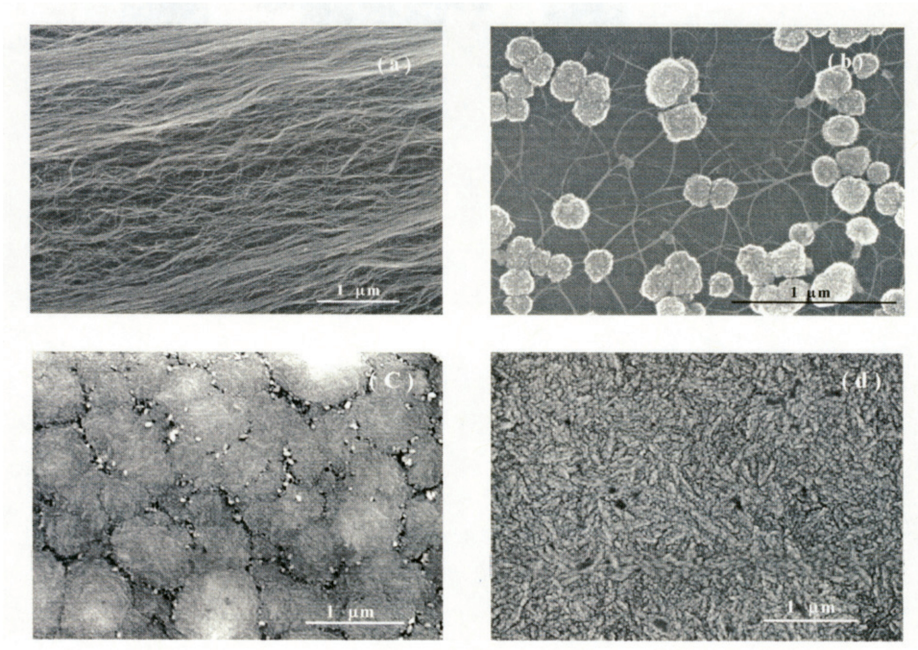

Figure 1. SEM pictures showing the evolution of the hybrid UNCD/CNTs structures via adjustment of the relative fraction of catalyst and nano diamond seeds. (a) Pure CNTs. (b) Hybrid structures of UNCD and CNTs, with lower fraction of CNTs and UNCD; (c) a nearly fully dense hybrid structure of UNCD and CNTs with high fraction of UNCD. (d) Pure UNCD.

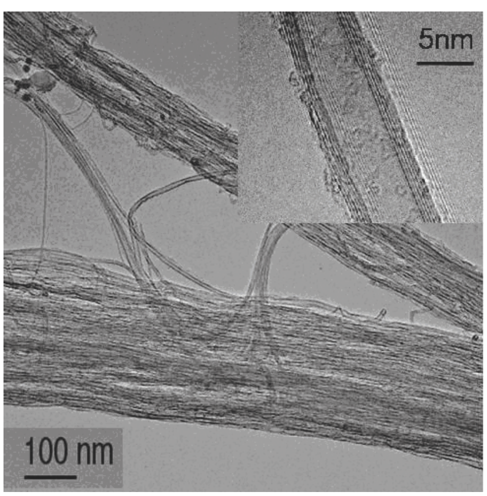

Figure 2. TEM images of CNTs prepared using PECVD with Ar /CH_4 as precursors. HRTEM shows that most CNTs were multi-walled with well-ordered grapheme sheets and typical defect densities.

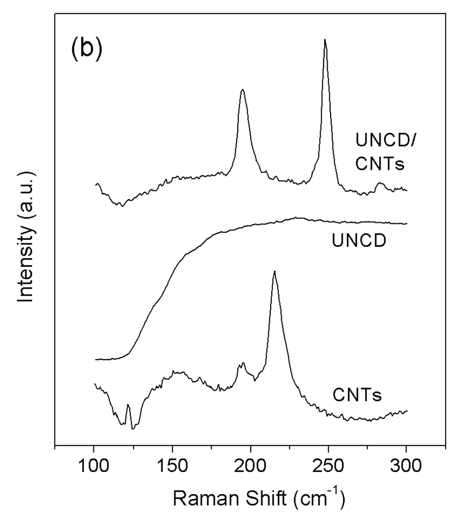

Figure 3. Raman spectra of CNTs, UNCD, and UNC/CNTs hybrid structures correspon-ding to the samples shown in Fig. 1a, 1b and 1d respectively.

Thermionic Field Emission from UNCD Coated Tip Structures

J. M. Garguilo, F. A. M. Koeck, *and* ***R. J. Nemanich,*** *North Carolina State University*
X. C. Xiao, O. Auciello, *and* ***J. A. Carlisle,*** *Argonne National Laboratory*

Motivation—Current studies involving thermionic energy converters point to crystalline carbon films in combination with field enhancing geometries as promising candidates for the emitting material. Thermionic energy conversion is accomplished through the combination of a hot electron emitter in conjunction with a somewhat cooler electron collector. In operation, an electric potential will develop between the two surfaces that can result in a significant source of electrical energy. The system converts the thermal energy into electrical energy. Since the process is based on electron emission and collection with no mechanical motion, this source can be highly efficient and operate without maintenance for extended periods of time. A limiting phenomenon to the vacuum emission of electrons is the space charge effect in which electrons in the vacuum close to the emitter surface impede additional electron emission. A method to combat this limiting effect is the introduction of surface features which produce a field enhancement effect at the surface. The electrons emitted from the tip shaped surface features are accelerated more rapidly across the vacuum gap to the electron collector.

Accomplishment—Ultra-nanocrystalline diamond (UNCD) films have been grown on etched silicon tip arrayed substrates. A thin metal layer separates the Si substrate and the diamond film. This metal layer enhances the pre treatment of the substrate which is critical for the nucleation of the diamond film. Raman spectroscopy of the films shows peaks consistent with typical UNCD films. SEM shows continuous coating of the underlying array and illustrates very clearly field enhancement geometry (Figure 1). Field emission electron microscopy (FEEM) measurements of the tip arrayed films give real time, spatially resolved images of thermionic field emission. The first significant emission above room temperature emission occurs at temperatures around and below 830º C. In this regime, an intense, temperature dependence is observed from both the tip structures of the sample as well as the flat, background areas (Figure 2). Field enhancement affects the intensity of emission resulting in brighter spots at the apex of the tips. This emission reaches its strongest around 830º C, rapidly degrading for temperatures in excess of this maximum. This temperature dependent degradation in emission has been observed for other nitrogen doped crystalline CVD films and is correlated to the desorption of surface bound hydrogen and the linked loss of the film's negative electron affinity (NEA). As the temperature is further increased, intense emission is once again observed from the tips of the sample (Figure 3). This emission is stable and cyclic and present only at the tips of the array. There is no contribution from the background.

Significance—Consistent field enhanced electron emission is crucial for thermionic energy converting devices. A limiting factor to the liberation of electrons in any thermionic energy converter is the screening of additional emission by vacuum electrons. Field enhanced electrons, compared to those emitted from a flat surface, will result in higher current densities at the collector. Thermionic energy conversion could, in principle, be a breakthrough answer to the power demands of the modern world because of the high efficiencies and low maintenance requirements inherent in the devices.

Contact: R. J. Nemanich, North Caroline State University
Phone: (919) 515-3225, Fax: (919) 515-7331, E-mail: robert_nemanich@ncsu.edu

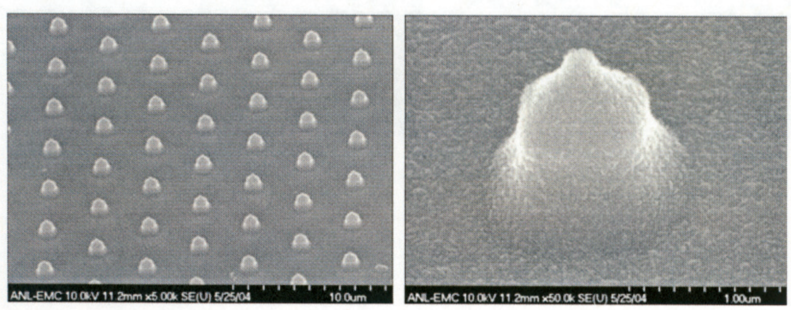

Figure 1. SEM images of the UNCD coated tip array. The uniform coverage of the substrate as well as the field enhancing geometry of the individual tips is clear.

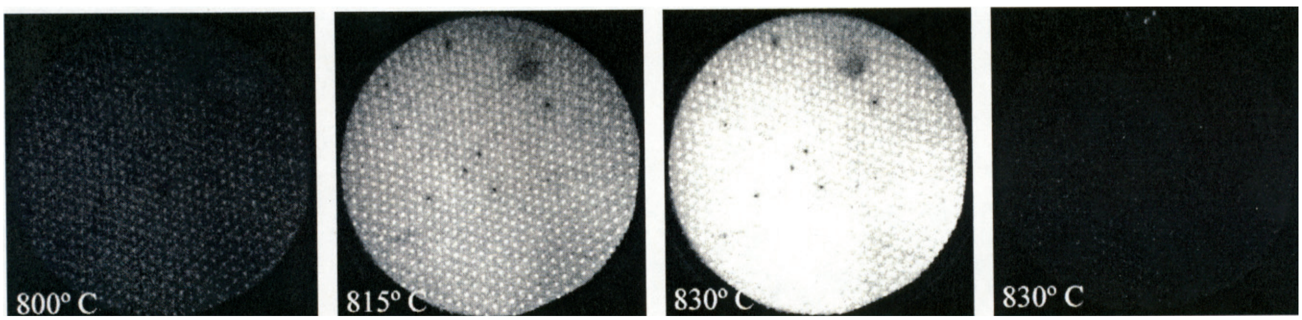

Figure 2. Temperature dependent FEEM images of the UNCD coated tip array. A steady increase in electron emission with increasing temperature is observed up to 830º C. Electron emission is detectable from both the tips and flat background of the sample. The geometric field enhancement effect results in stronger emission from the apex of the tips as compared to the background. After five minutes of exposure to the elevated (830º C) temperature, the emission degrades. This corresponds to a loss in the film's NEA due to hydrogen evolution from the surface.

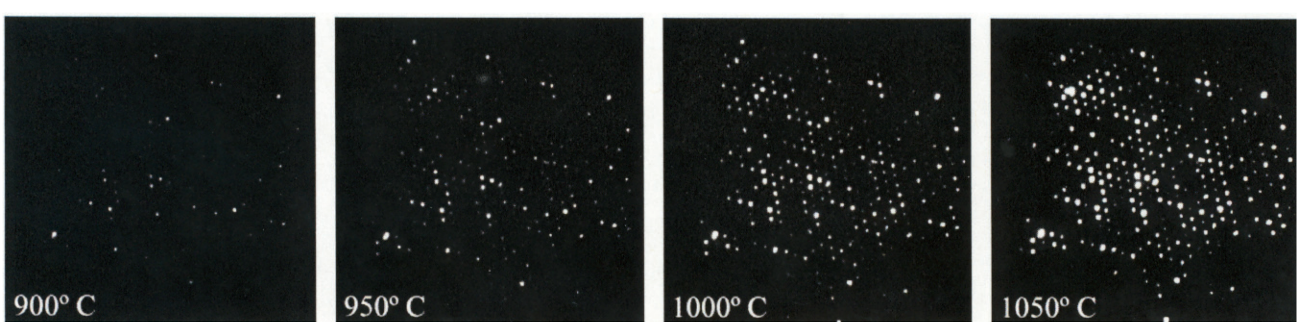

Figure 3. After the loss of the film's NEA, temperature dependent field emission continues to be present. As the sample is annealed to higher temperatures, strong electron emission is observed from the tips of the array. There is no longer detectable emission from the flat background of the sample. This emission is very stable and repeats with successive increasing and decreasing sweeps of the temperature.

Shear in Granular Couette Cells

Jeremy B. Lechman *and* ***Gary S. Grest,*** *Sandia National Laboratories, NM*
Antonio Barbero, Heinrich Jaeger *and* ***Sidney R. Nagel,*** *University of Chicago*

Motivation—Slow flows in dense granular materials are of practical in a variety of applications such as soil failure and powder processing, and as of yet are poorly understood. While progress has been made in understanding rapid flows in terms of kinetic theory, the nature of slow flows limits the use of such approaches. These denser systems often exhibit thin, localized regions of particle motion, shear bands, separating largely solid-like, immobile regions. To understand the flow in dense granular materials, we carried out a combined experimental and simulation study of flow in a split-bottom Couette cell as shown in Figure 1. Unlike traditional Couette cells with an inner wall that is rotated, an inner disk on the bottom of the cell is used to shear the system. This eliminates the need for an inner wall which can have a strong effect on the size of the shear zone.

Accomplishment—Using our parallel discrete element simulation code, it is now possible to model the same system sizes as in the experiment. As the fill height, H, of the particles in the cell increases, the width of the shear band increases and moves away from the outer wall. In Figure 2, results for azimuthal surface velocity in piles of various heights from both experiments using glass beads and discrete element simulations are shown. Similar results are found from simulations for the azimuthal velocity as a function of depth within a given pile. Moreover, these azimuthal velocities can be rescaled to fall on a universal curve regardless of the particle properties. This universal curve reveals excellent agreement between experiment and the simulation. The shape of this universal curve is found to be slightly asymmetric. We are presently investigating the origin of this asymmetry in more detail. When shearing shallow packs (R_s<H/2) the simulations exhibit an inner region which moves along with the bottom disk in a nearly solid-like fashion while the region between this inner core and a few particles lining the outer wall is fluidized. Snapshots of this inner core are shown in Figure 3 by removing "flowing" particles. Note the change in the shape and width as the height of the pile increases. For higher piles, this inner solid-like region disappears, as evident from Figure 2. The shape of this inner core is in qualitative agreement with a simple theoretical model based on Janseen's 1895 model of shear stresses in granular silos, which we investigated in previous studies. These results are also in agreement with NMR experiments using mustard seeds instead of glass beads to provide the required signal.

Significance—Using a new type of shear cell, we are able to study the development of the shear zone in dense granular flows. This cell has several advantages over the standard Couette cell. The width of the shear zone can grow arbitrarily large without interference from the boundaries, and the velocity profiles have a universal character independent of particle properties. This suggests that in a single system access to a range of flowing states can be gained, and fundamental questions about the nature of dense granular flows can be addressed. More precise measurement of the particle fluctuations can also be tracked either visually for motion on the surface or in the bulk by NMR. The simulations complement the experiments and give more detailed information on the structure of the pack and stresses than can be obtained experimentally. Future work includes studying the effect of cohesive interactions, such as moisture, on the shape of the shear zone.

Contact: Gary S. Grest, Sandia National Laboratories, NM
Phone: (505) 844-3261, Fax: (505) 844-9781, E-mail: gsgrest@sandia.gov

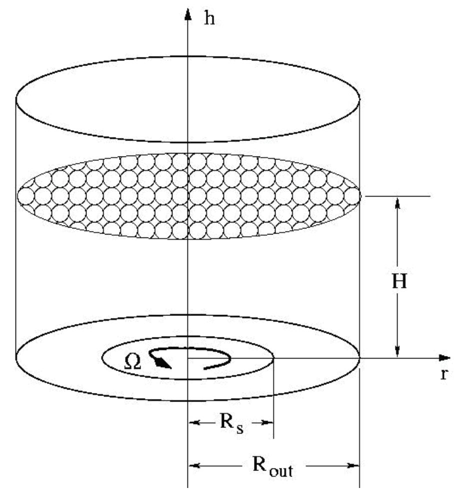

Figure 1. Schematic of split-bottom Couette system. Only the inner plate of radius Rs rotates. For the results presented here R_s=30d and R_{out}=39d, where d is the particle diameter.

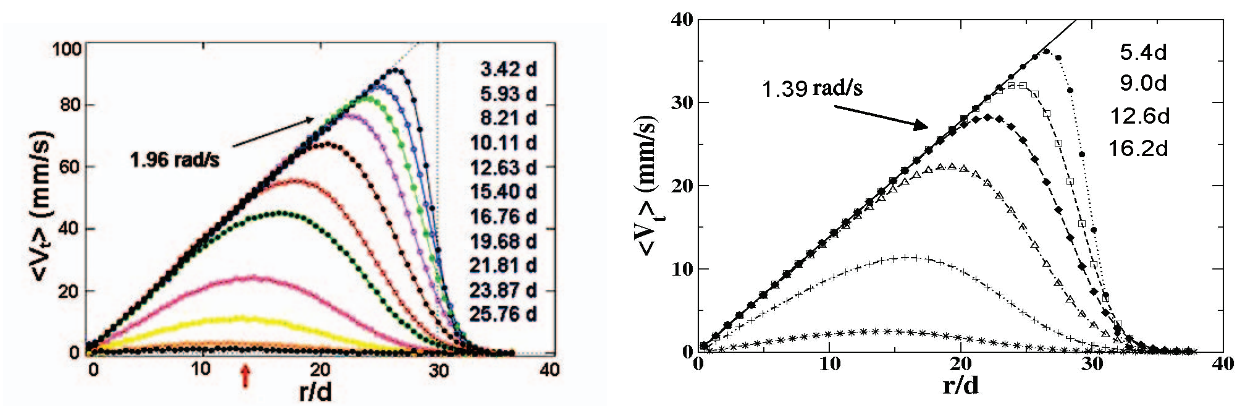

Figure 2. Azimuthal surface velocity profiles for packs of varying height in terms of particle diameter, d. Experimental result for glass beads (left), simulation (right).

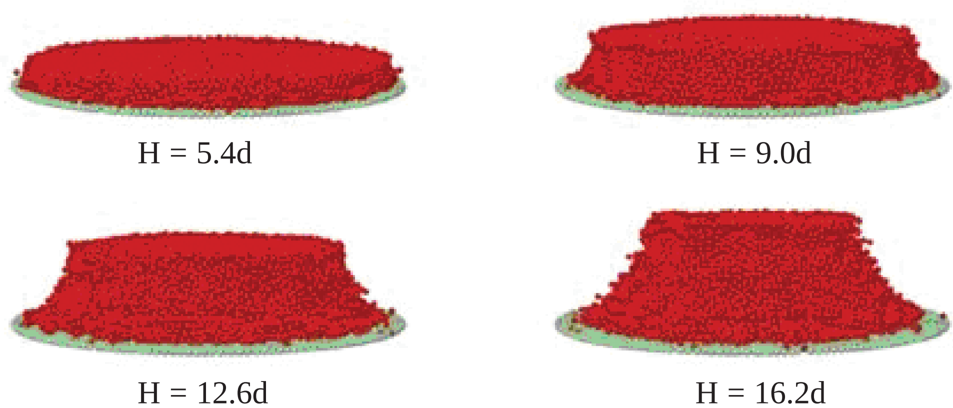

Figure 3. Snapshot of static inner core (red) particles determined by selecting particles which after ~1/4 revolutions had moved less than 0.005d in both h and r directions. Heights of the pile, H, are given in terms of the particle diameter, d.

Dynamics of Granular Flow on an Inclined Plane

Robert Ecke *and* ***Tamas Borzsonyi,*** *Los Alamos National Laboratory*
Thomas Halsey, *Exxon Mobil Research*
Igor Aronson, *Argonne National Laboratory*

Motivation—Granular flow on an inclined plane has become a model system for understanding how much the discreteness of a granular material affects continuum descriptions. Depth averaging and other continuum approaches have been quite successful in describing steady-state flow regimes and have been used as potential explanations for lateral structure formation in very fast flows on steep inclines. Another very interesting flow regime that we discuss here is the intermittent flow regime where spatially-localized avalanches of varying sizes and speeds are observed. We are interested in how the particle type affects the avalanche behavior. [1]

Accomplishment—We have measured the avalanche velocity and size for 4 different types and sizes of granular material including glass beads, two sizes of sand, salt and several kinds of copper powder materials. We find that the avalanches fall into one of two classes depending on the apparent interactions between the grains. Figure 1 shows the height profile of a granular avalanche obtained using a laser deflection method.

Most of the granular materials we used displayed an overturning type avalanche where the frictional or interaction forces were sufficiently high that when the avalanche begins the grains move faster than the front. The avalanches of this type are more than twice as high as the original layer depth and have ratios of fastest particle velocities to front speed of about 1.5. Glass beads avalanche via an entirely different mechanism. The beads induce progressive material failure of the weakly connected grains in front of the advancing avalanche causing a much slower and shorter avalanche. Avalanches of this type are typically only 50-60% higher than the layer depth and have a ratio of particle velocity to front speed of about 0.7. Figure 2 shows the velocity ratios for glass beads and for sand. A theory that takes into account individual granular particle rheology provides a quantitative model of the experiments.

Significance—The nature of avalanches in thin layers on inclined planes has been demonstrated to depend sensitively on the type of material in the avalanche. Analyzing the induced shear and the criterion for material failure provides a partial explanation for the avalanche behavior. More work to determine the underlying theoretical foundations for these surprising new results needs to be done.

1. T. Borzsonyi, T. Halsey and R. Ecke, submitted to Naure (2004).

Contact: Robert E. Ecke, Los Alamos National Laboratory
Phone: (505) 667-6733, Fax: (505) 665-2659, E-mail: ecke@lanl.gov

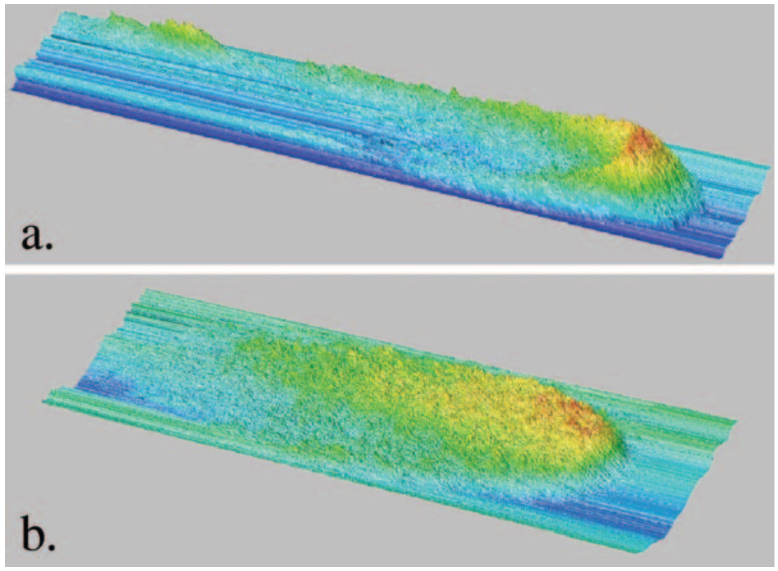

Figure 1. Height profiles of a) RNSG avalanche for θ=36.8°. Image size 7.2 cm x 56 cm, (vertical size rescaled by 25x) maximum height: h_m=0.34 cm, static layer thickness h_s=0.12 cm; b) SGB avalanche for θ=24.3°. Image size 12.2 cm x 46.8 cm, (vertical size rescaled by 25x) maximum height: h_m=0.29 cm, static layer thickness h_s=0.18 cm.

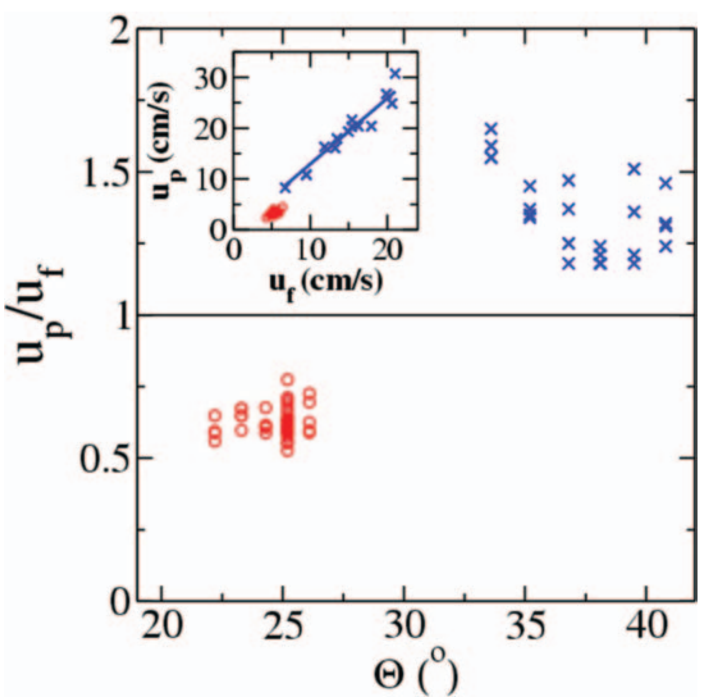

Figure 2. Ratio of particle and front velocities u_p/u_f for glass beads (o) and sand (x). The inset shows u_p vs u_f for θ=36.8° (sand) and θ=25.2° (glass beads).

Novel Behaviors in Electrostatically Driven Granular Media

Igor Aronson, Alexei Snezhko, *and* ***Maksim Sapozhniko,*** *Argonne National Laboratory*
Eli Ben-Naim *and* ***Avner Peleg,*** *Los Alamos National Laboratory*
Jeff Olafsen *and* ***Kevin Kohlstedt,*** *University of Kansas*

Motivation—Characterization of granular media is typically performed using mechanical driving. However, there are several drawbacks with such a driving: often it cannot be controlled with high precision and, additionally, the number of particles involved may be small, so statistical fluctuations are significant. This project uses charged micro and nano particles driven by an applied electric field to control the particle dynamics (Figure 1). The project combines experimental and theoretical capabilities with high speed imaging techniques to study dynamical and statistical properties of ensembles of fine powders.

Accomplishment—1) *Characterization of coarsening.* Electrostatically driven granular media in air or vacuum undergoes coarsening into growing immobile clusters of particles of circular shape. Using digital imaging techniques, we were able to characterize the cluster size distribution and its dynamics. The process is self-similar, i.e., throughout the system evolution, the size distribution is identical up to a change of scale. We developed a novel theory based on generalization of the celebrated Lifshitz-Slezov-Wagner approach to coarsening. The new element in the theory is incorporation of the binary coalescence between the clusters. Having zero fitting parameters, the theory gives a very good agreement with the cluster size distribution function (Figure 2).

2) *Characterization of velocity statistics in driven granular media with long-range interaction.* Using high-speed particle tracking methods, we measured the velocity distributions of electrostatically driven granular media with long-range interaction. The interaction was tuned either by immersing particles in non-polar dielectric fluid with adjustable viscosity, or by performing experiments with magnetic particles in external ac or dc magnetic field. In contrast to velocity distributions of conventional grains with short-range interaction ($P(v) \sim \exp[-v^{3/2}]$), the corresponding velocity distributions for magnetic particles, or particles in fluid, show much slower decay, $P(v) \sim \exp[-|v|]$. This anomalous behavior is explained in the framework of kinetic theory for the particles with long-range dipole interaction. We extended our studies to anisotropic particles (long dielectric rods) and observed a number of very interesting transitions resembling those of biological systems, such as ordering, formation of bundles, vortices etc, see Figure 3.

Significance—We have demonstrated that electrostatic driving is a controlled setting for driving granular media and that it allows precise and controlled characterization of granular ensembles. It can be successfully applied to systems of very small particles which cannot be controlled otherwise. Our coarsening results indicate that the structure of the cluster size distribution function is determined by the binary coalescence events. Our velocity measurements for the particles with non-local, long-range interaction indicates that the energy input from the boundary can be faithfully modeled by a thermal heat bath as the correlation between different energy input events is negligible. The anomalously slow decay of the distribution function at large velocities is determined by the dominant dipole interaction between the particles. Our preliminary studies with anisotropic rod-shaped particles revealed a great variety of new phenomena occurring in the electrostatically-driven system.

Contact: Igor Aronson, Argonne National Laboratory
Phone: (630) 252-9725, Fax: (630) 252-7777, E-mail: aronson@anl.gov

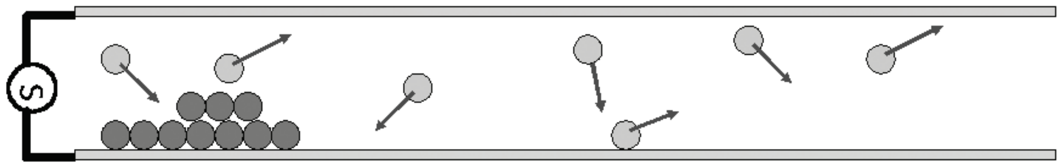

Figure 1. The experimental apparatus. Conducting microparticles are placed in the gap of a large capacitor. Particles are energized by ac or electric field in the following manner: particles pick the charge from the bottom electrode. If the electric force exceeds gravity, particles fly towards the upper electrode, recharge upon contact and falls down. Then the process repeats in a periodic fashion.

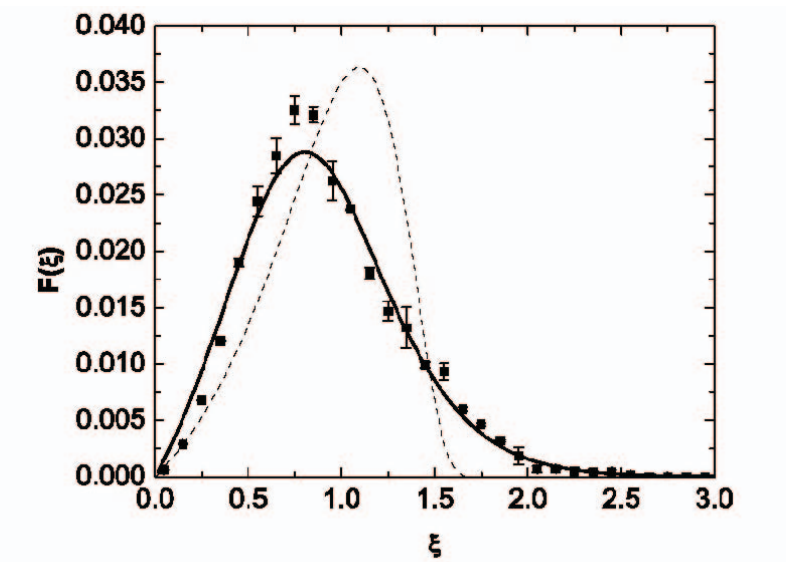

Figure 2. The cluster size distribution function in the coarsening dynamics in the electrostatically driven system of microparticles in ac electric field. The distribution presents an average of ~50,000 clusters formed by microparticles. Symbols show experimental results, Lifshitz-Slezov-Wager law is shown in dashed line, novel theory with binary coalescence is shown in solid line, no fitting parameters.

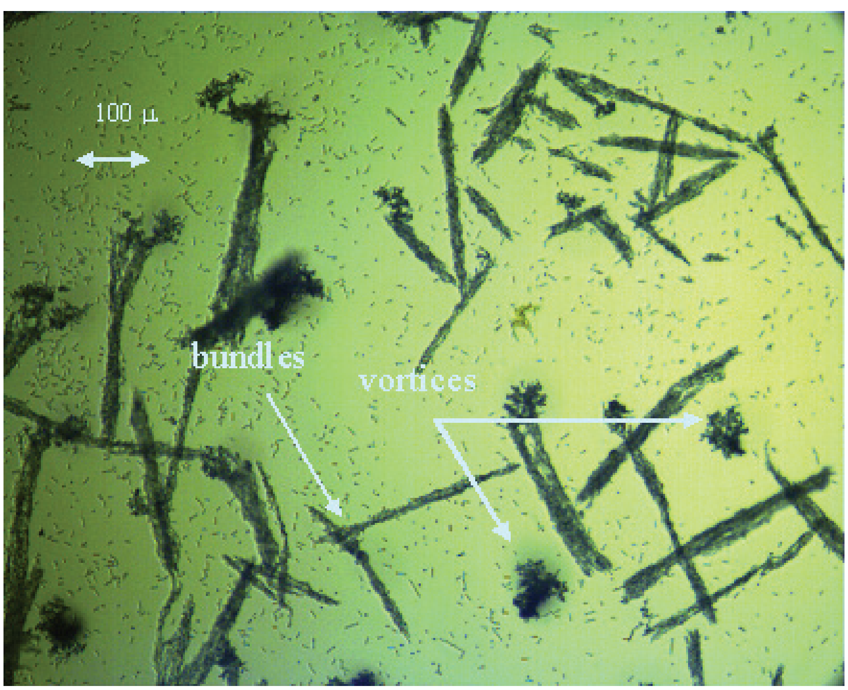

Figure 3. Formation of macroscopic oriented bundles in the system of electrostatically driven ceramic rods (average length 60 micron, diameter is approximately 5 micron) in a dielectric fluid (toluene). Upon application of dc electric field the rods self-assemble into long bundles due to long-range dipole electrostatic and hydrodynamic interactions. The bundles co-exist with the dynamic rotating vortices supported by self-induced electro-hydrodynamic flows.

Structure and Friction Dynamics of Hydration Layers Nanoconfined Between Mica Surfaces

Yongsheng Leng, *and* ***Peter T. Cummings,*** *Vanderbilt University/Oak Ridge National Laboratory*
Steve Granick, *Frederick Seitz Material Research Laboratory, University of Illinois*

Motivation—The structure, dynamics and shear properties of nanoconfined aqueous systems are of considerable interest in many areas such as clay swelling, colloidal stability, biolubrication and MEMS devices. Fluidity of hydration water in nanoconfinement between two mica surfaces has been recently observed down to a film thickness as small as approximately 1nm in surface force balance (SFB) experiments[1]. Further enhancement of shear viscosity (with orders of magnitude variation depending on wall alignment) was also observed for 1-2 water layers[2] through surface force apparatus (SFA). Understanding the lubricity of water is directly implicated in the development of micro/nano electromechanical systems (M/NEMS), as well as to fundamental advances in liquid state physics.

Accomplishment—At Vanderbilt/ORNL a nanotribological model in molecular dynamics (MD) simulation, as shown in Fig.1 was built up to mimic the shear dynamics of hydration layers in SFA/B experiments[3]. The molecular system includes the 2M1-muscovita mica, a typical 2:1 layered dioctahedral (hydroxy-) aluminosilicate, water molecules, and potassium ions K^+. We first investigate the hydration layer structure, particularly the density distributions along the normal direction of mica surfaces. This is shown in Fig. 2 where the MD simulation result of density oscillation of water oxygen is very similar to the X-ray reflectivity experiment[4]. We observed the adsorbed and hydration peaks of water molecules adjacent to the mica surface, which are the basic features observed in X-ray reflectivity experiments by Fenter's group[4].

Complementary measurements[3] of aqueous solutions down to 1-2 water layers at the FS/MRL found shear enhancement and shear viscosity varied by many orders of magnitude depending on the two mica surfaces alignment. In MD simulations, shearing of water films in the MD regime showed that the hydrated potassium ions still attach to the mica surfaces, and there are no significant stick-slips. Shear viscosity enhancement (~42cP) in the Newtonian regime is observed for three-layer water films (D=0.92nm), beyond which shear viscosity of hydration water is very close to the bulk value (Fig. 3). Further decrease in film thickness of hydration water down to 1~2 water layers leads to significant viscosity increase, as has been observed - the 'shear thinning' in MD regime. This issue is still under investigation.

Significance—Current experimental and theoretical efforts in the investigation of the structure and friction dynamics of nanoconfined hydration water will enhance our understanding of constrained aqueous fluids in many naturally occurring systems, such as biological and nanomechanical systems. The ultimate goal is the realization of friction control in M/NEMS and biological system.

1. U. Raviv and J. Klein, Science **297**, 1540 (2002).
2. Y. X. Zhu and S. Granick, Phys. Rev. Lett. **8709** (2001).
3. Y. S. Leng and P. T. Cummings, Phys. Rev. Lett. **94, (In the press)** (2005).
4. L. Cheng, P. Fenter, K. L. Nagy, et al., Phys. Rev. Lett. **87**, 156103 (2001).

Contact: Yongsheng Leng, Vanderbilt University
Phone: (615) 322-8793, Fax: (615) 343-7951, E-mail: yongsheng.leng@vanderbilt.edu

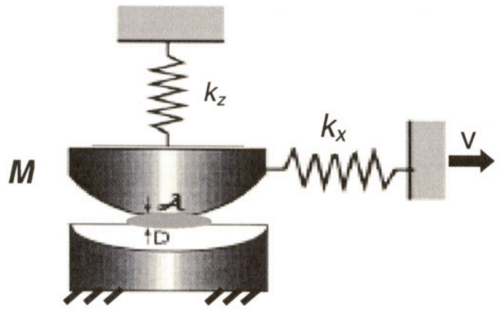

Figure 1. Schematic model in MD simulations to mimic the friction dynamics in SFA(B) experiments.

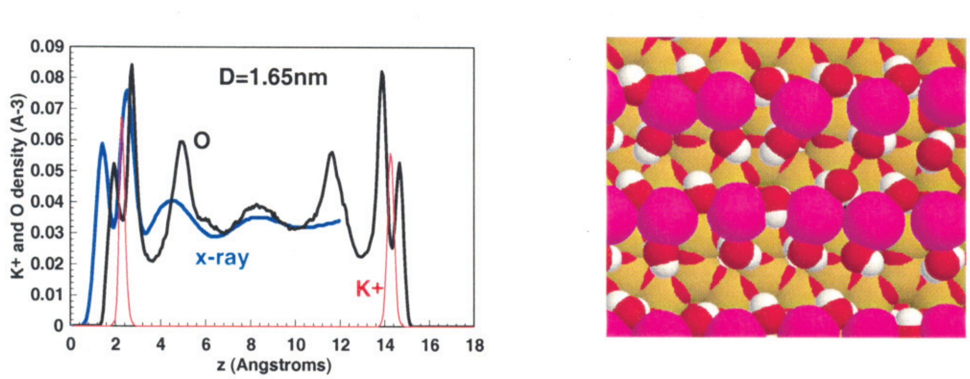

(a) (b)

Figure 2. (a) Water oxygen (O) and potassium ion K^+ density distributions adjacent to mica surfaces. The first small 'peak' corresponds to adsorbed water layer. (b) Viewing the water-mica surface from above, adsorbed water molecules are found to be attached to the ditrigonal cavities of mica surface with their dipoles pointing inward to the centers of rings. Potassium ions, which originally sit on the ditrigonal cavity before being hydrated by water, are displaced right above the tetrahedral Al (not visible).

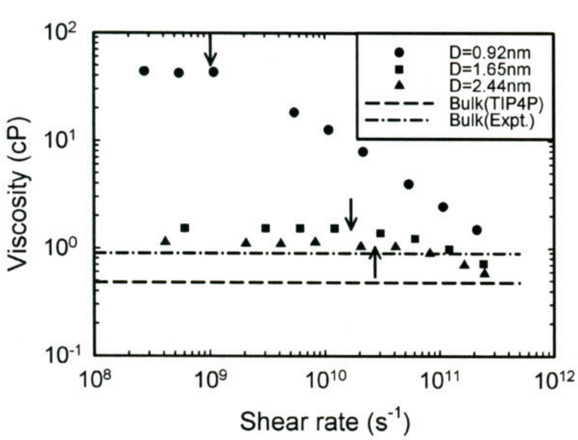

Figure 3. The variations of shear viscosity versus shear rate for different hydration layers and the bulk water in a log-log scale. The Newtonian plateau for D=0.92nm hydration layer is calculated to be 0.042Pa·s. The error bars of shear viscosity at very low shear rates (the last three data) are less than 10% (i.e., less than the size of curve symbol). At larger shear rates the error bars are even smaller (less than a few percent).

Using Friction to Produce Materials

Steve Granick, *Frederick Seitz Materials Research Laboratory, University of Illinois*
Miquel Salmeron, *Lawrence Berkeley Laboratory*

Motivation—In the studies summarized here, we employ friction not as a phenomenon against which remedies are needed, but rather as a constructive tool that can be employed to synthesize materials under gentle conditions of temperature and pressure that otherwise would be incompatible with the desired outcome. The context is that molecularly-thin films of fluids are ubiquitous in boundary-layer lubrication, friction in MEMS devices, and numerous other applications where the large ratio of surface to volume renders friction an unusually large issue. Better understanding of these issues could lead to improvements in the rational remediation of friction and wear problems, as well as to fundamental advances in liquid state physics.

Accomplishment—The transformation of a random coil into a squeezed, directionally-aligned conformation thinner than random coil dimensions is usually studied in the context of friction forces. Instead, one can use frictional sliding as a processing tool to induce other properties. To illustrate this concept, at the FS/MRL we considered optical properties of the conjugated polymer, MEH-PPV (poly(2-methoxy-5-(2-ethylhexyloxy)-1,4-phenylenevinylene) end-capped with dimethyl phenyl), selected because of its potential applications in optoelectronic devices (Fig. 1). Dilute solutions of this polymer were introduced into a surface forces apparatus, allowed to adsorb, then confined to a thickness (2 nm) roughly 20 percent of the unperturbed dimension of the molecules, forcing alignment parallel to the confining single crystal surfaces. Large-amplitude oscillatory shear imparted additional directional alignment. The photoluminescence and absorption spectra of the dry polymer films showed that chains were shear-oriented with interesting consequences for the optical properties (Fig. 2). The manipulation of molecular structure by frictional sliding offers a simple and generalizable method to control chain conformations at the nanoscale.

Complementary studies at LBNL addressed the structure, conformation, and electronic properties of oligothiophenes. Of particular significance was to understand how their self-assembly and packing structure control electronic transport along the thiophene chain Friction was observed to alter the packing orientation. The electronic properties were observed to depend on the load applied by an AFM tip. For improved molecular-level control of electronic properties, enabling new ideas were develop by which to use friction to organize molecule-electrode configurations.

Significance—Extreme deformations are most apt to happen in thin films of soft materials because molecular motions and relaxations are tremendously retarded by adsorption and confinement. Thus, it easily happens that molecules are deformed more rapidly than they can re-equilibrate. This can be applied to identify simple, generalizable approaches by which to capitalize on friction of molecularly-thin films to control useful materials properties. This was illustrated by showing how optoelectronic properties were modified by combined alignment of chain conformations by shear and confinement to slits thinner than random-coil dimensions. We also anticipate that novel chemical reactions may transpire after reactant molecules have been confined and oriented by frictional sliding.

Contact: Steve Granick, Frederick Seitz Materials Research Laboratory, University of Illinois
Phone: (217) 333-5720; Fax: (217) 244-2278; E-mail: sgranick@uiuc.edu

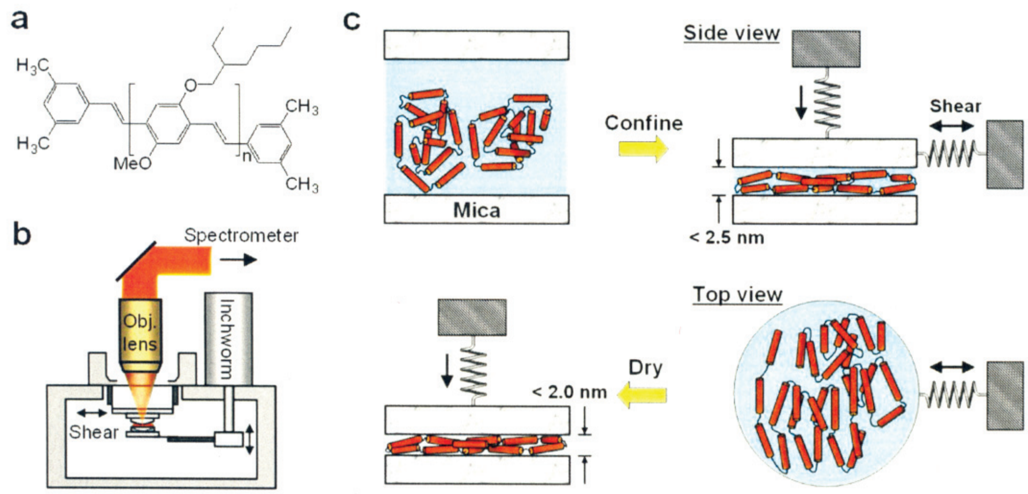

Figure 1. Experimental scheme. The conjugated polymer, MEH-PPV (a) was dissolved in dilute toluene solution at concentration 0.5 mg-mL^{-1}. After loading into a surface forces apparatus adapted for photoluminescence studies (b), the solution was squeezed under an applied load to nanometer thickness, sheared, and dried (c). The shear perturbations were sinusoidal at 1.3 Hz with large amplitude, 15 times the final film thickness (33 nm rms amplitude). This caused the electronic structure of the ultrathin film, denoted in the diagram by red cylinders, to align preferentially perpendicular to the shear direction.

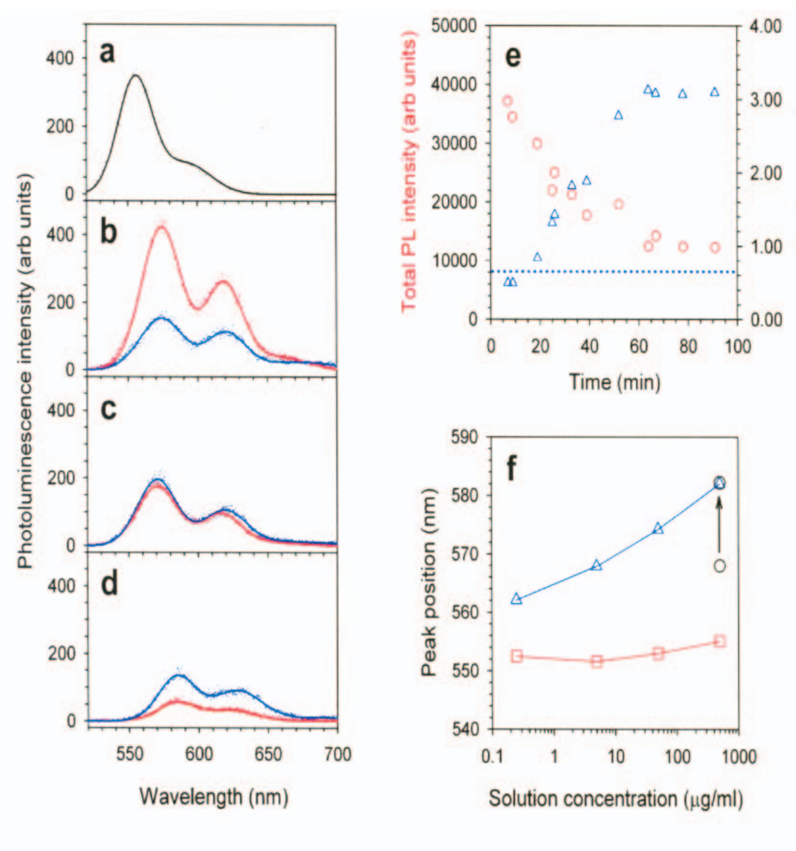

Figure 2. Photoluminescence spectra of films 2.0±0.2 nm thick. (a) shows PL spectra of bulk solution for comparison. Illustrative PL data, polarized parallel and perpendicular to incident light, which was also the shear direction (red and blue, respectively) are plotted after 7, 25, and 130 minutes (b, c, and d, respectively). In d, the film is dry. (e) shows integrated intensity (circles) and intensity ratio, perpendicular to parallel (triangles) plotted against time sheared; the dotted line characterizes the latter in bulk solution. (f) shows concentration dependence of the peak wavelength of the 0 $\rightarrow$ 0 transition for MEH-PPV solutions of various concentration in solution (squares), in films dried without shear (triangles), a film 2 nm thick under shear with residual solvent (circle) and this latter film dried (at end of the vertical arrow).

Fundamental Tribology of Micromachines Across Length Scales

R. W. Carpick, M. D. Street, *and* ***E. E. Flater,*** *University of Wisconsin-Madison*
M. P. de Boer *and* ***A. D. Corwin,*** *Sandia National Laboratories, NM*

Motivation—Any device, experiment, or application that contains rubbing components will possess interfaces that experience energy dissipation (friction) and inevitably, interfacial damage (wear). At small scales, the surface- or interface-to-volume ratio strongly increases, and these interfacial interactions become dominant. This is a critical issue in micro-electromechanical systems (MEMS), where interfacial adhesion-, friction- and wear-related tend to be the dominant failure mechanisms. The primary goal of this study is to determine and understand the fundamental behavior of friction in micromachine interfaces by working across length scales (Fig. 1). A "nanotractor" device with well-defined and controlled frictional interfaces has been designed and fabricated at Sandia.

Accomplishment—Our experiments have revealed clear correlations between MEMS tribological performance and the molecular architecture of lubricating self-assembled monolayers . For octadecyl trichlorosilane (OTS) and octadecene (Fig. 2, left), which are both surface-micromachining compatible, we see that nanotractor friction is lower for OTS than octadecene (Fig. 2, center).

In a joint experiment, AFM measurements of fundamental frictional interactions at the single asperity scale *using the same interfacial materials and coatings* as the nanotractor have revealed strong contrasts between the two different molecular coatings (Fig. 2, right). The data are fit well using adhesive contact mechanics models showing friction is proportional to the true contact area through a shear strength whose pressure dependence depends on the molecule. The difference between OTS and octadecene may be related to different molecular packing and ordering in the films. Surprisingly, while octadecene exhibits higher friction at the MEMS level, it exhibits *lower* friction in the AFM measurements. The key is the difference in pressure and wear regimes: the AFM experiment is carried out in a low-pressure, elastic (damage-free) regime. Indeed, at the highest loads, we see that friction in octadecene becomes comparable to OTS (Fig. 2, right). Experiments at higher pressure to match the damage-creating regime in the MEMS devices are under way.

We observed that tailoring the surface roughness (from 3 to 10 nm rms) has a small effect on the wear life, while monolayer lubricant coatings had a more pronounced effect. The nano-scale roughness was quantitatively evaluated using a contact model to make predictions regarding the tendency to produce wear. The initial nanoscale surface roughness is indeed predicted to create high contact stresses that could lead to wear, while the worn surfaces possessed atomically smooth features that lead to low contact pressures, consistent with steady-state sliding. This suggests that MEMS wear may be reduced with sub-nanometer surface roughness.

Significance—We are finding that the integrated, multi-scale study of friction using both AFM and MEMS-level experiments can reveal new insights into friction, adhesion, and wear in these devices. We anticipate applying these results to provide mechanism-based design rules for high-performance MEMS systems.

Contact: R. W. Carpick, University of Wisconsin-Madison
Phone: (608) 263-4891, Fax: (608) 263-7451, E-mail: carpick@engr.wisc.edu

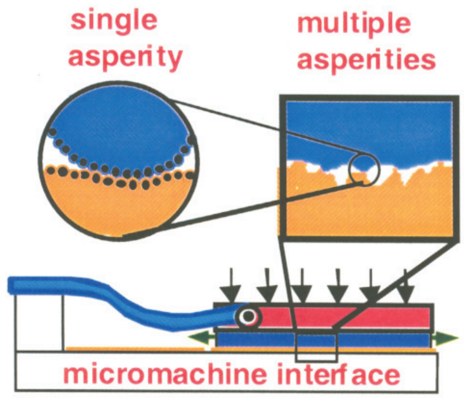

Figure 1. A MEMS test device investigates multi-asperity interfaces (up to 1 mm by 2 µm in size). AFM studies controlled single-asperity contacts of the same materials (<5 nm across).

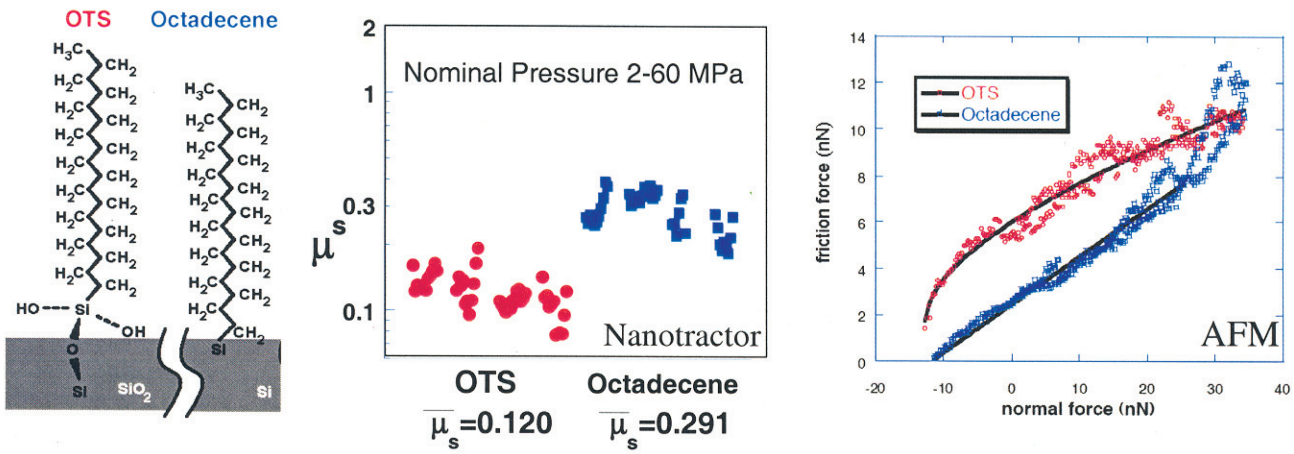

Figure 2. Left: molecular structure of OTS and octadecene. Center: Nanotractor results. Right: AFM single asperity friction measurements. The solid lines show fits of continuum mechanics models to the data.

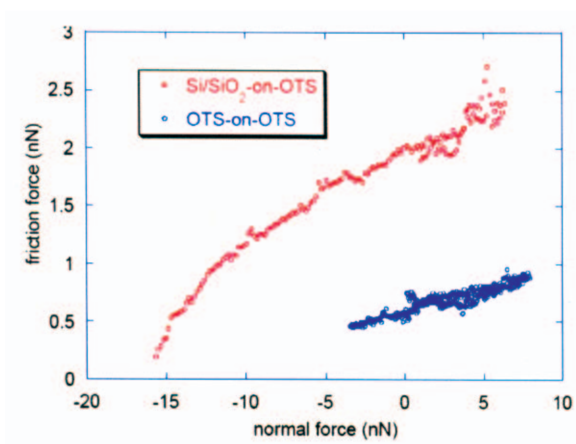

Figure 3. Friction measurements between an uncoated SiO2 tip and OTS has dramatically higher friction and adhesion than an OTS tip on a OTS surface.

Full Bulk Spin Polarization and Intrinsic Tunnel Barriers at Manganite Surfaces

J. W. Freeland, K. E. Gray, L. Ozyuzer, P. Berghuis, E. Badica, J. Kavich, H. Zheng, *and* ***J. F. Mitchell,*** *Argonne National Laboratory*
J. Eckstein, *University of Illinois Urbana-Champaign*

Motivation—Transmission of information using the spin of the electron as well as its charge (spintronics) requires a high degree of spin polarization (SP) at surfaces. At surfaces, however, competing interactions, chemical inhomogeneity, and strains or surface reconstruction can quench this degree of polarization. Many half-metallic ferromagnetic (FM) oxides exhibit very high bulk magnetization, but the SP at surfaces and interfaces declines more rapidly than the bulk magnetization as the Curie temperature, T_c, is approached. Our CSP partner Freescale Semiconductor stresses that a high degree of SP allows a higher device density because of improved signal-to-noise, motivating our quest to improve surface SP and to understand it.

Accomplishment—Using a combination of surface sensitive x-ray and tunneling probes, we show for the quasi-two-dimensional bilayer manganites $La_{2-2x}Sr_{1+2x}Mn_2O_7$ that the outermost Mn-O bilayer, *alone*, loses SP. This 1-nm thick intrinsic nanoskin (see Fig. 1) is an insulator with no long-range FM order, while the next bilayer displays the full SP of the bulk.

By tuning circular-polarized x-rays to the Mn L edge, resonant magnetic scattering (XRMS) and absorption (XMCD) reveal the magnetization profile near the surface by subtracting data for different helicity. A comparison of such data to calculation in Fig. 2 shows unambiguously that only the single surface bilayer lacks FM order. In stark contrast to all other half-metallic oxides, the temperature dependence of the SP in the second bilayer replicates the bulk magnetization found by neutron scattering. This comparison is shown in Fig. 3, which also shows that SP degrades with temperature even for high-quality MBE-grown perovskite manganite films (Fig. 3 inset).

The electronic properties were probed with gold-tip point contacts that can only exhibit tunneling if an insulating barrier is present on the surface of the crystal. The limiting current-voltage characteristics, after repeatedly cleaning the surface, are indicated by the three data sets of Fig. 4. Note that both polarities are shown and the higher current is for the manganite positive. That all three data sets fit tolerably well to the calculation of tunneling (lines), over a range of 10,000 in current, indicates a highly uniform barrier of height 375 meV and width ~1.4 nm. This width coincides with the distance between the second (metallic) Mn bilayer and the gold tip (Fig. 1).

Significance—This research has demonstrated the natural self-assembly of two-thirds of an ideal magnetic tunnel junction. The layered manganites are the first example of a half-metallic, FM oxide that exhibits virtually full bulk SP *at the junction interface*. The barrier is perfectly uniform and self-protecting with an additional advantage of a small height to promote high current density and minimize noise. The inevitable defects in heterogeneous barriers can depolarize tunneling currents by spin-flip scattering, but the homogeneous natural barrier essentially excludes this possibility. The quest to complete this ideal magnetic tunnel junction is the natural next step for this project.

Contact: J. F. Mitchell, Argonne National Laboratory
Phone: (630) 252-5852, Fax: (630) 252-7777, E-mail: mitchell@anl.gov

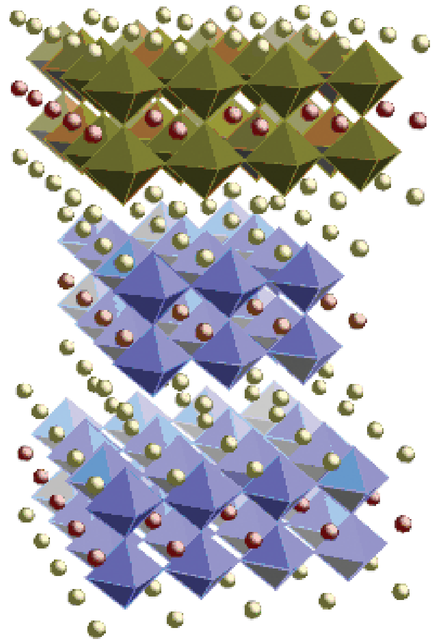

Figure 1. Structure of a bilayer manganite with a nonmagnetic surface layer indicated in brown.

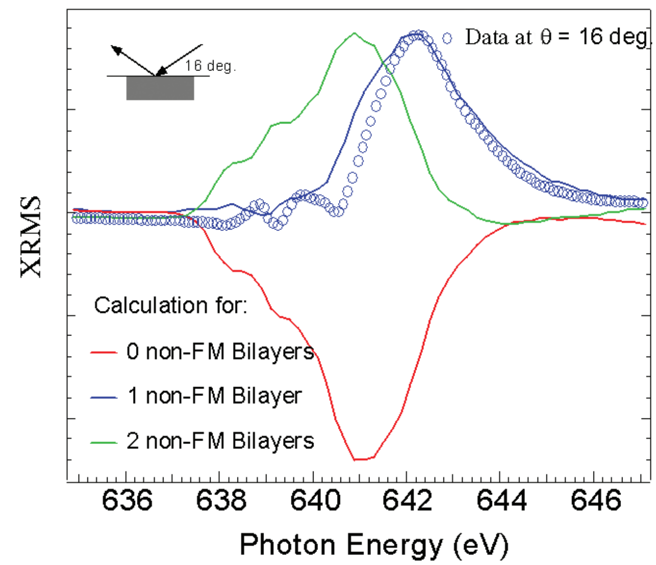

Figure 2. Clear signature in x-ray resonant magnetic scattering (XRMS) of the loss of magnetization only in the surface bilayer.

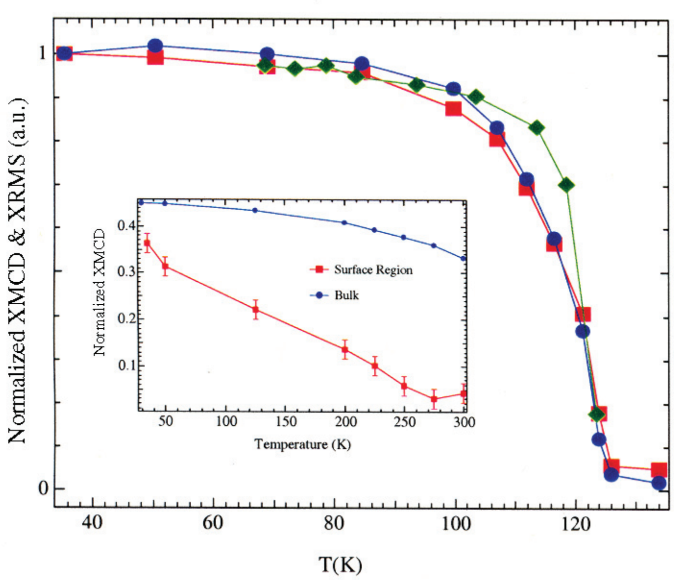

Figure 3. Surface polarization (XRMS and XMCD) of the bilayer manganite follows the bulk magnetization as T_C is approached. (Blue: XRMS, Red: XMCD, Green: bulk magnetization). The inset shows the contrasting behavior of a perovskite manganite thin film grown by MBE.

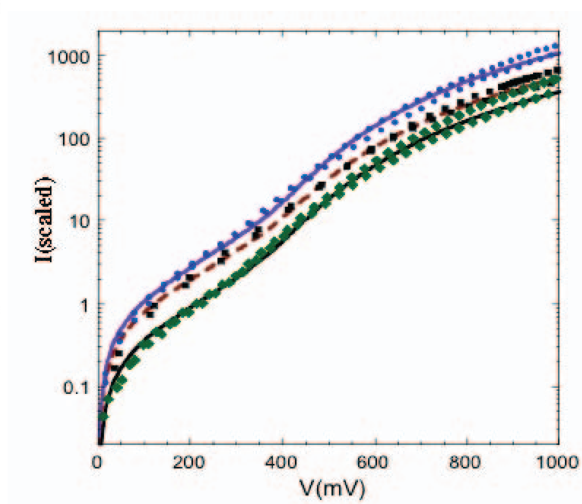

Figure 4. Point-contact tunneling data taken at 4.2 K represent the limiting behavior after the surface has been cleaned by the gold tip, and they fit very well to the tunneling calculation (bold lines) for a barrier height of 375 meV and width 1.4 nm.

Does Double Exchange Explain One-Dimensional Manganite Nano-Wires?

J. N. Eckstein, M Warusawithana, X. Zhai, *and* ***J. O'Donnell,*** *University of Illinois*
J. Freeland, *Argonne National Laboratory*

Motivation—Manganites exhibit a wide range of properties, and even within compositions that are ferromagnetic there are a number of factors that control magnetism, the metal insulator transition and the nature of the charge carriers. All of the phases are similar in their structure and can be grown in thin film form on a range of substrates. Strain in these layers changes the critical temperature and the magnetoresistance and can lead to substantial magnetocrystalline anisotropy. This complexity has motivated us to learn how to combine different manganite phases into heterostructures where the interfaces dominate transport and magnetism. While interesting results have been obtained in layered structures, zero-dimensional and 1-D nanostructures offer the possibility of increasing the importance of interfaces on aggregate properties. In this work we have developed a method of growing 1-D wires of one perovskite phase $La_{0.7}Sr_{0.3}MnO_3$ (LSMO) embedded in a film of a second perovskite phase $La_{0.7}Ca_{0.3}MnO_3$ (LCMO).

Accomplishment—LSMO in thin film form has a T_c of > 330 K, while tensile strained LCMO has a T_c of ~160 K. We find that the wires order magnetically at a substantially different temperature than the metal insulator transition (MIT) temperature By choosing the embedding material to have a lower critical temperature and metal insulator temperature than the wire material, we also have obtained highly anisotropic transport. Figure 1 illustrates the form of the structures we have grown. This is obtained by starting with a substrate miscut in a direction perpendicular to the direction of the wires. After a film of the embedding material is grown, a half of a monolayer of the wire material is deposited. This is followed by a short anneal period during which time the RHEED intensity recovers, indicating the accumulation of a half a monolayer at the step edge. This is followed by the growth of half a monolayer of the embedding phase which again is followed by a short anneal period. By accurately repeating this process, a vertical superlattice is grown with a pitch controlled by the terrace length which itself is determined by the miscut angle. We have grown on substrates with terrace lengths of 100 nm and 15 nm. The wires grown on the first sample were 50 nm in diameter. Because the transport is constrained in a direction perpendicular to the wire, the LSMO wire material magnetically orders at a relatively high temperature, although suppressed from the bulk T_c. This is shown in figure 2. The second lower temperature transition is due to the LCMO matrix material which is substantially suppressed by tensile strain. (All of these films are clamped to the substrate lattice.) The spatially separated two phases together give rise to anisotropic transport. Figure 3 shows that conduction along the direction of the wires is substantially easier than perpendicular to the wires. This is also evident in nonlinear transport. Perhaps the most puzzling aspect of our data is the large separation indicated in figure 3 between the higher magnetic ordering temperature and the MIT temperature. Usually these are very nearly the same, but in these structures they are substantially different.

Significance—The possibility of combining different manganite phases in accurately assembled 1-D nanostructures with new magnetic textures was demonstrated. We shall next study the magnetic structures obtained in this way and use these films in magnetotransport devices such as spin valve tunnel junctions.

Contact: J. N. Eckstein, University of Illinois
Phone: (217) 244-7709, Fax: (217) 244-2278, E-mail: eckstein@uiuc.edu

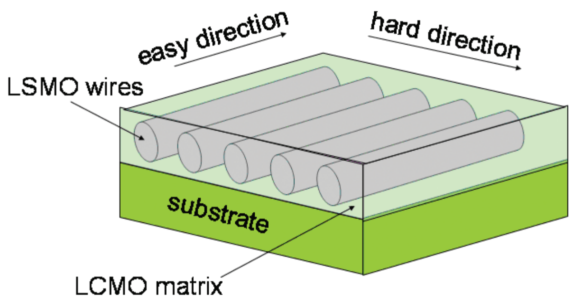

Figure 1. Structure of 1-D nanowires of LSMO embedded in an LCMO matrix. The pitch of the wires (100 nm for the results shown here) is controlled by the substrate miscut angle.

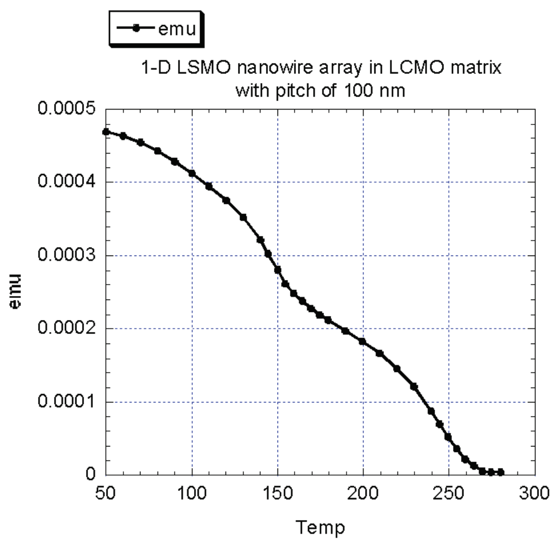

Figure 2. Two magnetic transitions seen in a nanowire sample. The higher transition temperature is in the wire, while the lower transition is in the matrix material. LCMO is known to exhibit a T_c in the range of 160 K when grown in tension on $SrTiO_3$.

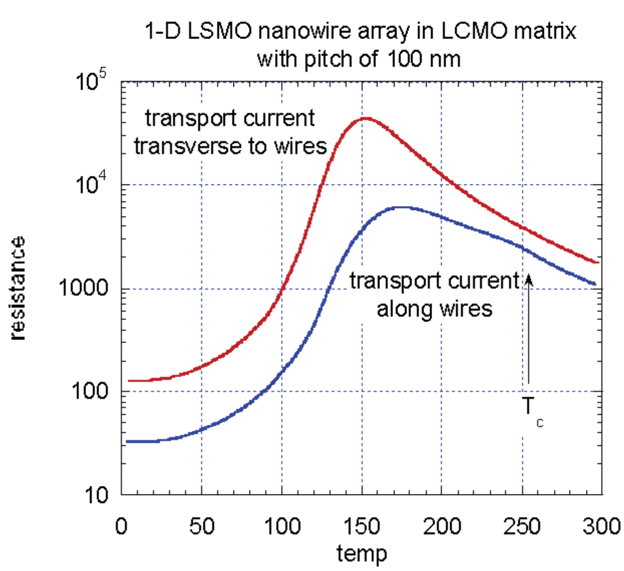

Figure 3. Anisotropic transport in 1-D LSMO nanowire sample. Transport along the wires has lower resistance and exhibits a temperature dependence modified by the presence of the insulating LCMO. The magnetic (T_c) and transport (peak) transition temperatures for the LSMO parts of the film are dramatically different.

Ultrasharp Magnetization Steps in Phase Segregated Manganite Films

J. F. Mitchell *and* ***T. Wu,*** *Argonne National Laboratory*

Motivation—Achieving highly spin-polarized carriers in manganites will require highly homogeneous materials, as spin polarization will degrade in the presence of impurities, second phases, etc. Manganites are known to exhibit complex phase competition between ferromagnetic metal (FMM) and anti-ferromagnetic insulating (AFM-COI) phases on differing length scales. To understand the impact of such inhomogeneity, we have investigated the temperature and field behavior of an intentionally-made inhomogeneous material in film form. The role of strain on the transition between AFM-COI and FMM is particularly salient, as this strain may in principle be manipulated through substrate epitaxy.

Accomplishment—Ultrasharp steps have been observed in bulk phase segregated manganites at low temperature. The mechanism behind such ultrasharp steps has been attributed to catastrophic relief of strain built up during the first-order martensitic phase transition between these competing states. In order to explore the generality of such sharp metamagnetic transitions and the potential impact of extrinsic strain, we have studied thick (700 Å - 7000 Å) $Pr_{0.65}(Ca_ySr_{1-y})_{0.35}MnO_3$ (PCSMO) films at low temperature. In this system, the volume fraction of AFM-COI to FMM varies with y, and *T* (Fig 1). This phase fraction is also highly *H*-dependent, as highlighted in Fig. 2a, which shows that all films exhibit metamagnetic behavior associated with the conversion of CO-AFM phase to FM phase. However, the appearance of sharp steps in these films depends sensitively on the measurement protocol. When the magnetization is measured by a typical field sweep, the steps occur *only* in thick (> 0.5 µm) y=0.8 films, which have the largest AFM-COI volume fraction. However, the sharp steps absent in the other films during these typical magnetization measurements can be recovered by holding the sample at fields near the metamagnetic transition field (H_c) for periods of minutes to hours.(Fig. 2b). This constant temperature, constant field onset of sharp steps is consistent with an "induction period," during which strain fields are presumably self-organizing and FMM volume fraction is slowly growing in parallel. Additionally, as shown in Fig 3, evidence of small steps can be observed even for $H \ll H_c$ transition field. The latter finding indicates that a metastable hierarchy of magnetization states exists in the films connected both by slow (exponential) and abrupt (step-like) transitions. We note that in these thick films the impact of the substrate is expected to be small. It is apparent from this study, however, that the strain states and their mechanism of relaxation in the epitaxial film differs from the bulk analogs.

Significance—The interplay of AFM-COI and FMM states is critical to current models of CMR manganite physics. Our results in films show that, while the steps are intrinsic to the physics of these materials, the time over which strain fields organize can be significantly impacted by the sample form and magnetic history. This suggests that control of such features may be feasible by establishing appropriate strain states in the as-made film.

Contact: J. F. Mitchell, Argonne National Laboratory
Phone: (630) 252-5852, Fax: (630) 252-7777, E-mail: mitchell@anl.gov

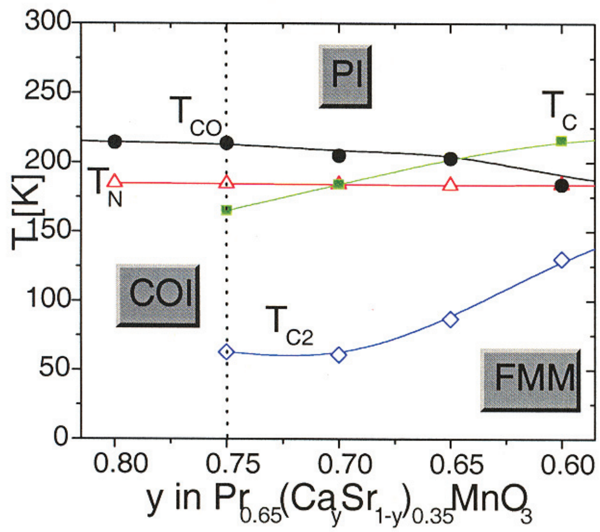

Figure 1. Competing phases in bulk $Pr_{0.65}(Ca_ySr_{1-y})_{0.35}MnO_3$ determined by neutron powder diffraction. T_{co} is the charge-ordering temperature, T_c is the Curie temperature, T_N is the Neel temperature, and T_{c2} represents the temperature at which the ferromagnetic phase grows rapidly at the expense of the CO phase.

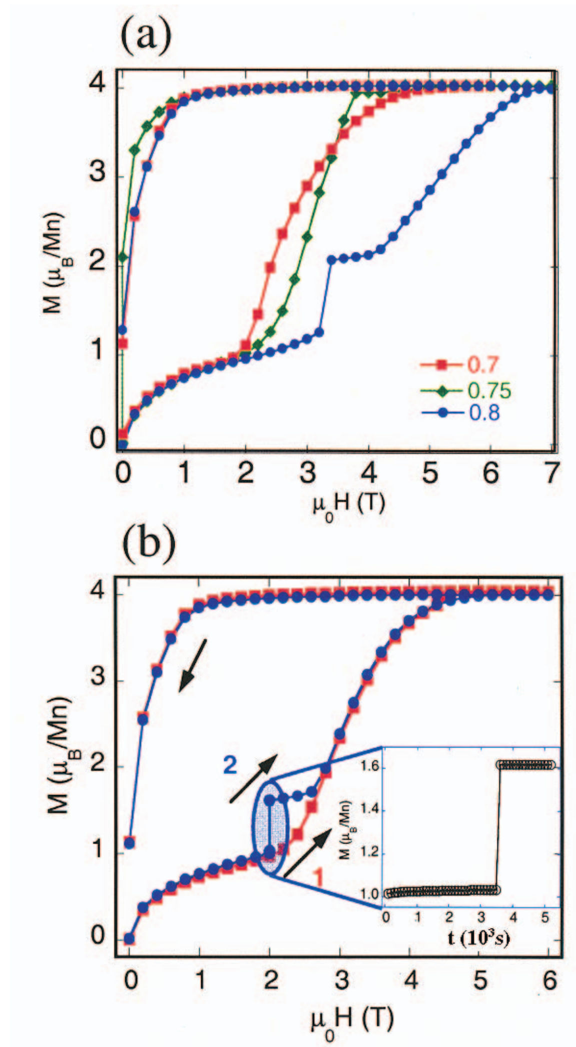

Figure 2. Magnetization of $Pr_{0.65}(Ca_y,Sr_{1-y})_{0.35}MnO_3$ films at 2 K. (a) Normal sweep mode showing metamagnetic transitions for all films, with a sharp step for y=0.8 (b) Comparison of normal sweep (path 1) to interrupted sweep (path 2) for a y=0.7 film in which no step is seen for path 1. In path 2, the field was raised to 2 T then held for several minutes. The inset shows that the sharp step appears after ~1 hr hold time.

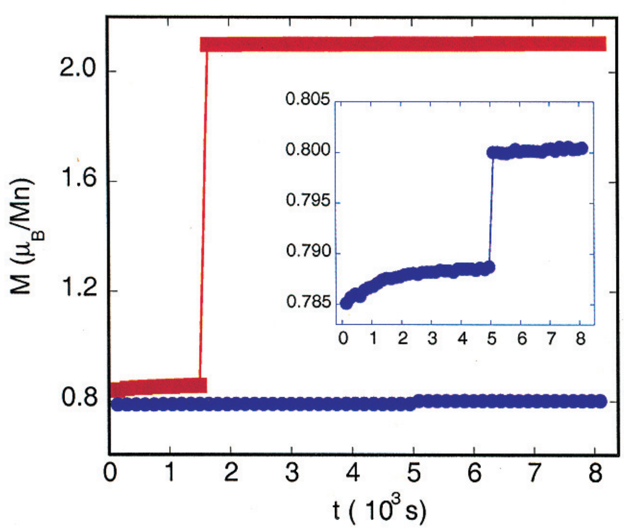

Figure 3. Comparison of time-dependent magnetization for y=0.7 film after ramping to 1 T (blue) or 2 T(red). The inset shows an expanded view of the 1 T data. For times less than the step, the magnetization can be fit to a stretched exponential form.

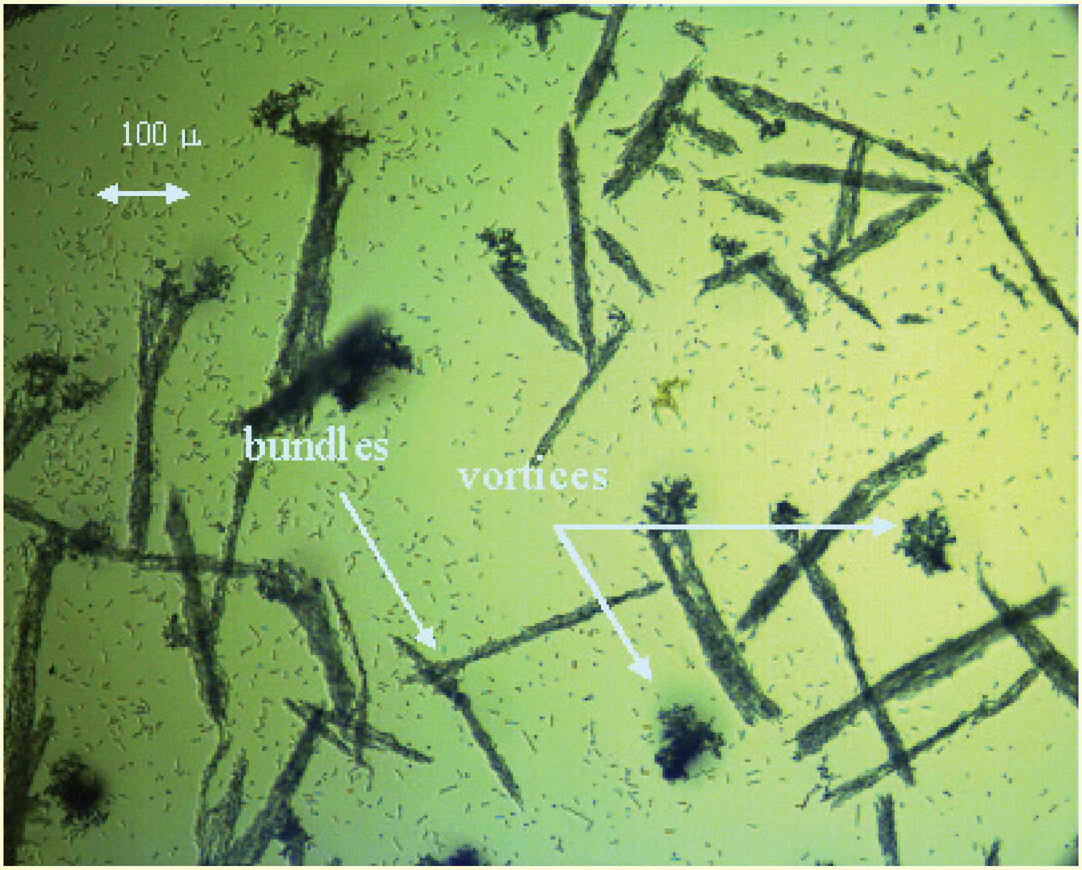

The figure on the front is a schematic depiction of a random collection of uniaxial magnetic particles in an applied magnetic field. Exchange coupling between the nanograins in nanostructured permanent magnet materials can enhance the energy product by up to 50% (see p. 18).

The above image shows the formation of microscopic bundles of electrostatically-driven ceramic rods in a dielectric fluid. Upon application of a *dc* electric field the rods self assemble into long bundles due to long-range dipolar electrostatic and hydrodynamic interactions (see p. 44).

SAND2005-0671P: Prepared by the DOE Center of Excellence for the Synthesis and Processing of Advanced Materials at Sandia National Laboratories, Albuquerque, New Mexico 87185 for the Division of Materials Sciences and Engineering, Office of Basic Energy Sciences, U.S. Department of Energy. Sandia is a multiprogram laboratory operated by Sandia Corporation, a Lockheed Martin Company, for the Department of Energy's National Nuclear Security Administration under Contract No. DE-AC04-94AL85000.

Printed in October 2004